# Single cell RNA sequencing unravels the transcriptional network underlying zebrafish retina regeneration

Laura Celotto[1], Fabian Rost[2], Anja Machate[1], Juliane Bläsche[2], Andreas Dahl[2], Anke Weber[1], Stefan Hans[1], and Michael Brand[*1]

[1] Technische Universität Dresden, CRTD - Center for Regenerative Therapies Dresden, Center for Molecular and Cellular Bioengineering (CMCB), Fetscherstraße 105, 01307 Dresden, Germany

[2] Technische Universität Dresden, DRESDEN-Concept Genome Center, Center for Molecular and Cellular Bioengineering (CMCB), Fetscherstraße 105, 01307 Dresden, Germany

*Corresponding author

ORCID: Laura Celotto: 0000-0002-9191-4056; Fabian Rost: 0000-0001-6466-2589; Andreas Dahl: 0000-0002-2668-8371; Anke Weber: 0000-0003-2220-658X; Stefan Hans: 0000-0003-0283-0211; Michael Brand: 0000-0001-5711-6512

Keywords: Retina, regeneration, zebrafish, Müller glia, progenitors, light lesion, scRNAseq

## SUMMARY

In the lesioned zebrafish retina, Müller glia produce multipotent retinal progenitors that generate all retinal neurons, replacing lost cell types. To study the molecular mechanisms linking Müller glia reactivity to progenitor production and neuronal differentiation, we used single cell RNA sequencing of Müller glia, progenitors and regenerated progeny from uninjured and light-lesioned retinae. We discover an injury-induced Müller glia differentiation trajectory that leads into a cell population with a hybrid identity expressing marker genes of Müller glia and progenitors. A glial self-renewal and a neurogenic trajectory depart from the hybrid cell population. We further observe that neurogenic progenitors progressively differentiate to generate retinal ganglion cells first and bipolar cells last, similar to the events observed during retinal development. Our work provides a comprehensive description of Müller glia and progenitor transcriptional changes and fate decisions in the regenerating retina, which are key to tailor cell differentiation and replacement therapies for retinal dystrophies in humans.

## INTRODUCTION

The vertebrate retina is the neural tissue in the back of the eyes that detects and processes visual stimuli prior to transmission to the brain (Dowling, 1987). The retina has a layered structure, with outer, inner and ganglion cell nuclear layers alternating with the outer and inner plexiform layers (Amini et al., 2018; Hoon et al., 2014; Stenkamp, 2015). The nuclear layers comprise the nuclei of retinal neurons, whereas the plexiform layers contain neuronal synapses. There are six distinct classes of retinal neurons and one main type of glia: retinal ganglion, cone photoreceptor, horizontal, amacrine, rod photoreceptor and bipolar cells, as well as Müller glia. This heterogeneity

48 arises during development in the indicated order from a common pool of multipotent
49 retinal progenitor cells (RPCs), which progressively restrict their competence to
50 generate early and mid-late born cell fates (Agathocleous and Harris, 2009; Alexiades
51 and Cepko, 1997; Amini et al., 2018; Cepko, 2014; Cepko et al., 1996; Livesey and
52 Cepko, 2001; Stenkamp, 2015, 2007; Turner and Cepko, 1987; Weber et al., 2014;
53 Young, 1985). Retinal development, structure and function are highly conserved
54 among vertebrates, including the teleost zebrafish (*Danio rerio*) with only slight
55 variations. For instance, humans and zebrafish possess a cone-dominated retina
56 adapted for diurnal visual tasks, whereas nocturnal animals, like mice and rats, have
57 rod-dominated retinae adapted for a dim light lifestyle (Fleisch et al., 2011; Saade et
58 al., 2013; Stenkamp, 2007). Intriguingly, and in contrast to warm-blooded vertebrates
59 like birds and mammals, adult zebrafish can fully regenerate their retinae upon lesions
60 affecting different neuronal cell types, depending on the injury paradigm. For instance,
61 intense light ablates preferentially light-sensing rod and cone photoreceptors in the
62 central and dorsal retina, whereas application of neurotoxins, like ouabain or NMDA,
63 affects mainly retinal ganglion and amacrine cells (Bernardos et al., 2007; Fimbel et
64 al., 2007; Powell et al., 2016; Sherpa et al., 2008; Vihtelic et al., 2006; Vihtelic and
65 Hyde, 2000; Weber et al., 2013). Independently of the lesion type, Müller glia (MG),
66 acting as resident stem cells, are the primary cellular origin of regenerated cells.
67 Specifically, zebrafish MG react to the lesion by partial dedifferentiation and cell cycle
68 re-entry, followed by an asymmetric division producing renewed MG and multipotent
69 RPCs (Gorsuch and Hyde, 2014; Lahne et al., 2020b; Lenkowski and Raymond, 2014;
70 Wan and Goldman, 2016). Dedifferentiation of MG to a progenitor-like state is not
71 complete, as MG upregulate progenitor-associated genes like *pax6* or *vsx2*, but retain
72 their glial morphology. In this context, glial markers like Glial Fibrillary Acidic Protein
73 (*gfap*) as well as glutamine synthase (*glula*) have been reported to be either retained

74 or downregulated, depending on the lesion paradigm, the regeneration time point, the
75 antibody and the transgenic line used to label MG (Fimbel et al., 2007; Lenkowski and
76 Raymond, 2014; Nagashima et al., 2013; Thummel et al., 2008). However, in all
77 reported cases, MG-derived RPCs do not express *gfap* (Lenkowski and Raymond,
78 2014; Thummel et al., 2008). Asymmetric cell division of MG occurs between 31 hours
79 and 2 days post-lesion, followed by further proliferation of MG-derived RPCs that peaks
80 at 4-5 days post lesion, depending on the injury paradigm (Bernardos et al., 2007;
81 Fausett and Goldman, 2006; Fimbel et al., 2007; Nagashima et al., 2013). Studies on
82 zebrafish retina regeneration have so far mainly focused on very early phases of MG
83 dedifferentiation and RPC production (Fausett et al., 2008; Nelson et al., 2013;
84 Ramachandran et al., 2011, 2010; Thummel et al., 2010, 2008; Wan et al., 2012; Zhao
85 et al., 2014). Recent work showed that MG initially assume a reactive state,
86 characterized by the expression of *hmga1a* and *yap1*, prior to giving rise to
87 proliferative, neurogenic RPCs (Hoang et al., 2020). Consequently, impaired Yap1 or
88 Hmga1a function impedes MG reprogramming and neurogenesis in the regenerating
89 retina (Hoang et al., 2020). In contrast, the molecular and cellular identities of self-
90 renewed MG and MG-derived RPCs remain elusive. RPCs have fusiform nuclei that
91 closely associate with GFAP-positive glial fibers across the inner nuclear layer. They
92 also express markers of multipotency, like Pax6 and Sox2, as well as markers of
93 neurogenesis, like Atoh7 (Fausett and Goldman, 2006; Gorsuch et al., 2017;
94 Nagashima et al., 2013; Raymond et al., 2006; Thummel et al., 2010). Previous studies
95 have investigated RPCs molecular identity mainly at the population level (Cameron et
96 al., 2005; Hoang et al., 2020; Kassen et al., 2007; Kramer et al., 2021; Lahne et al.,
97 2020a; Morris et al., 2011; Ng Chi Kei et al., 2017; Powell et al., 2016; Qin et al., 2009;
98 Ramachandran et al., 2012; Thummel et al., 2008). However, a detailed
99 characterization of the transcriptional network underlying RPC production and RPC

differentiation, as well as the lineage relationships between MG, RPCs and differentiating progeny is currently missing. Here, we profiled the transcriptome of MG and MG-derived RPCs in response to an intense light lesion, and followed their differentiation trajectories towards regenerated retinal neurons at the single cell level. In particular, we addressed the transcriptional state of reactive MG prior to and after their asymmetric cell division. Moreover, we addressed whether MG-derived RPCs are heterogeneous and to what extent they express molecular markers that are observed during embryonic retinogenesis (Xu et al., 2020). To this aim, we employed a short-term lineage tracing strategy that allowed the isolation of individual MG and MG-derived cells of the regenerating zebrafish retina, which were subsequently subjected to droplet-based, 10x Genomics single cell RNA sequencing (scRNAseq). We find that MG can be non-reactive in uninjured and lesioned conditions, as well as reactive upon lesion. Reactive MG give rise to a hybrid cell population, which replenishes the pool of MG as well as feeds into the pool of neurogenic RPCs. Moreover, MG-derived RPCs are highly heterogeneous and display a progressive restriction in their competence during subsequent differentiation. They upregulate developmental markers of retinogenesis and produce regenerated neurons partially according to the developmental birth order, with retinal ganglion cells born first and bipolar cells born last.

## RESULTS

### Isolation of individual MG, RPCs and regenerated progeny using fluorescent reporters

124 Previous work on the regenerating zebrafish retina described the early phases of MG
125 de-differentiation and RPC production (Cameron et al., 2005; Fausett et al., 2008;
126 Fausett and Goldman, 2006; Lahne et al., 2015; Nagashima et al., 2013; Nelson et al.,
127 2013; Thummel et al., 2010). However, knowledge on the molecular identity and cell
128 fate choices of RPCs is scarce and based on analyses at a population level (Cameron
129 et al., 2005; Hoang et al., 2020; Kramer et al., 2021; Lahne et al., 2020a; Ng Chi Kei
130 et al., 2017; Powell et al., 2016; Qin et al., 2009; Ramachandran et al., 2012; Thummel
131 et al., 2008). To study MG activation, RPC identity and their relationship with MG in
132 more detail, we profiled the transcriptome of MG and MG-derived RPCs and followed
133 their differentiation trajectories towards regenerated retinal neurons at the single cell
134 level. To do so, we devised a strategy to isolate individual MG, RPCs and regenerated
135 progeny, using retinae of uninjured and light-lesioned fish carrying the two fluorescent
136 reporters *pcna:EGFP* and *gfap:mCherry*. The former drives the expression of EGFP
137 under the regulatory elements of *proliferating cell nuclear antigen* (*pcna*), a known
138 marker of proliferating cells, and thereby labels actively dividing cells, and, due to the
139 persistence of EGFP, their short-term progeny. The other reporter drives expression
140 of mCherry under the regulatory elements of *glial fibrillary acidic protein* (*gfap*), a
141 known marker of zebrafish MG. Both transgenes recapitulate the endogenous
142 expression in the adult zebrafish retina faithfully (Figure1-figure supplement 1).
143 Immunohistochemistry against the proliferation marker PCNA co-labeled *pcna:EGFP*-
144 positive cells mainly in the ciliary marginal zone, one of the stem cells niches in the
145 adult zebrafish retina (Bernardos et al., 2007; Raymond et al., 2006). Occasionally,
146 *pcna:EGFP*/PCNA-double positive cells were observed in the central retina as well
147 (Figure1-figure supplement 1A). The MG-specific antibody Zrf1 labeled virtually all
148 *gfap:mCherry*-positive cells in the central retina as well as in the ciliary marginal zone
149 (Bernardos et al., 2007) (Figure1-figure supplement 1B). We also addressed the

150 expression of the two fluorescent reporter lines following light lesion, at three different
151 time points upon injury. First, 44 hours post light lesion (hpl), when MG are about to
152 undergo or have already completed their asymmetric cell division giving rise to the first
153 RPCs and self-renewed MG (Lahne et al., 2015; Nagashima et al., 2013). Second, 4
154 days post light lesion (dpl), representing the peak of RPC proliferation (Bernardos et
155 al., 2007; Fausett and Goldman, 2006) and third, 6 dpl, when the first differentiating,
156 regenerated progeny arise (Bernardos et al., 2007). Immunohistochemistry against
157 EGFP and mCherry in double transgenic *Tg(pcna:EGFP);Tg(gfap:mCherry)* animals
158 corroborated the expected expression pattern of the transgenes in the central retina at
159 the chosen time points (Figure1-figure supplement 2). Uninjured, central retinae
160 displayed no EGFP, but strong mCherry signal consistent with non-proliferating MG
161 (white arrowheads). In contrast, numerous EGFP/mCherry double-positive cells were
162 present at 44 hpl, indicating potential cell-cycle re-entry of MG (yellow arrowheads). At
163 4 dpl, overall mCherry expression was reduced, consistent with the previously
164 described downregulation of the *gfap* promoter by MG-derived RPCs. In contrast,
165 EGFP was strongly found throughout all retinal layers, matching the reported peak in
166 proliferation of MG-derived RPCs (red arrowheads) (Bernardos et al., 2007; Fausett
167 and Goldman, 2006; Fimbel et al., 2007; Lenkowski and Raymond, 2014; Thummel et
168 al., 2008). Finally, in comparison to 4 dpl, an increase in mCherry accompanies a
169 decline in EGFP signal at 6 dpl (yellow arrowhead). In order to obtain single cells of
170 MG, RPCs and regenerated progeny, we utilized the persistence of EGFP and
171 mCherry fluorescence, providing a short-term label. Initially, only MG express mCherry
172 in uninjured, central retinae, but activate EGFP in preparation of the asymmetric cell
173 division upon light lesion at 44 hpl (Figure 1A). Firstborn RPCs inherit high levels of
174 persisting fluorescent mCherry protein from dividing MG and slowly degrade/dilute the
175 protein during subsequent rounds of cell division. Hence, MG-derived, but further

176 dividing, RPCs are EGFP-positive, but low mCherry-positive at 4 dpl. At 6 dpl, RPCs
177 have further diluted the mCherry reporter, thus displaying only a faint mCherry signal,
178 but remain EGFP-positive. Similarly, RPC-derived, regenerated progeny is
179 characterized by even lower levels of intrinsic mCherry fluorescence, and low EGFP
180 signal during subsequent cell differentiation at 6 dpl. Following this rationale, we
181 dissected retinae of uninjured and light-lesioned samples, dissociated them into single
182 cell suspensions that were subjected to flow cytometry followed by droplet-based, 10x
183 Genomics scRNAseq (Figure 1B). Flow cytometry plots confirmed the rationale of the
184 above-mentioned strategy (Figure 1C and Figure1-figure supplement 3). In all
185 samples, we detected non-fluorescent and EGFP-positive only cells, consistent with
186 non-proliferating and proliferating cells in the adult zebrafish retina. We also detected
187 cell populations expressing only mCherry at all sampled time points, most likely
188 representing non-reactive MG. In addition to cells expressing either EGFP or mCherry,
189 we find EGFP/mCherry-double positive cells in all samples consistent with proliferating
190 MG originating from the ciliary marginal zone and the central retina (see Figure1-figure
191 supplement 1 and 2). The EGFP/mCherry-double positive population increased at 44
192 hpl, presumably due to an increase in the cell number of reactive, proliferating MG. At
193 4 dpl, the expanded EGFP/mCherry-double positive cell population was still present,
194 but displayed a lower mCherry, yet an increased EGFP signal, in line with MG-derived
195 RPCs, peaking in proliferation (Bernardos et al., 2007; Fausett and Goldman, 2006).
196 At 6 dpl, a further decreased mCherry intensity was observed for the EGFP/mCherry-
197 double positive cell population. In order to profile the transcriptome of individual MG,
198 RPCs and progeny of the uninjured and light lesioned retinae, we dissected retinae of
199 the before-mentioned time points (uninjured, 44 hpl, 4 dpl, 6 dpl) and eventually sorted
200 15.000 cells per time point. We applied a sorting gate that included both mCherry-
201 positive only and EGFP/mCherry-double positive cells at the sampled time points

202 (Figure 1C and Figure 1-figure supplement 3). Non-fluorescent as well as EGFP- only
203 positive cells were not included. Taken together, we devised a short-term lineage
204 tracing strategy that allows the isolation of individual MG and MG-derived cells of the
205 regenerating zebrafish retina, which can be subjected to droplet-based,10x Genomics.

206

207 **scRNAseq identifies 15 distinct cell populations in the light-lesioned retina**

208 Sorted cells underwent 10x Genomics scRNAseq and 13.139 cells passed the
209 sequencing quality control. We detected a median of 1.407 genes and 4.061 mean
210 read counts per cell. Initially, we identified three clusters for the full dataset (Figure 2-
211 figure supplement 1A): a retinal core dataset and two additional clusters identified as
212 microglia and low-quality cells expressing many ribosomal transcripts (Figure 2-figure
213 supplement 1B). Both populations were excluded from the subsequent analysis. Re-
214 clustering of the core dataset, which eventually included 11.690 cells, revealed 15
215 potential, different cell populations (Figure 2A). From left to right on the UMAP, which
216 visualizes the cell lineage trajectory, we observed the progressive emergence of MG,
217 RPC and progeny clusters. We assigned the cellular identity by inspecting the top 100,
218 upregulated marker genes per cluster (supplementary file 1). In detail, we identified
219 four MG clusters (clusters 1 to 4) that locate to the left and middle portion of the map,
220 followed by five RPC clusters (clusters 5 to 9) locating to the right side of the map.
221 Regenerated progeny branch from the RPCs and include retinal ganglion (cluster 10),
222 amacrine (cluster 13) and bipolar cells (cluster 15) at the bottom-right, as well as red
223 and blue cones (clusters 11 and 12) at the top-right of the map. Additionally, there is a
224 second cluster of amacrine cells (cluster 14) that separates from the first amacrine cell
225 cluster.

226 To investigate how the composition of cells changed during regeneration, we
227 computed embedding densities for each time point (Figure 2B). Similar to the
228 progression of cellular identities, cells progressed over time from left to right, from the
229 uninjured, to the 44 hpl, the 4 dpl, as well as the 6 dpl enriched samples. As expected,
230 cells belonging to non-reactive MG were found at all sampled time points. In particular,
231 the vast majority of cells of the uninjured sample belonged to cluster 1 as well as cluster
232 2. However, we also observed a small proportion of cells (Figure 2B) aligning in a
233 trajectory from non-reactive MG (left side of the map) through reactive MG (middle
234 part) to RPCs and differentiating progeny (right side) in the uninjured sample. At 44
235 hpl, cells mapping to non-reactive MG were still abundantly present, although mostly
236 shifted right towards a cluster representing reactive MG (cluster 3). Cells belonging to
237 this cluster of reactive MG were also highly enriched in this sample. In contrast, cells
238 mapping to the second cluster of reactive MG (cluster 4) as well as to RPCs (clusters
239 5-9) were overrepresented at 4 dpl, in line with the reported peak in proliferation at this
240 time point (Bernardos et al., 2007; Fausett and Goldman, 2006). Cells mapping to
241 RPCs were still frequently present at 6 dpl. Moreover, cells belonging to regenerated
242 progeny (clusters 10-15), which first appear at 4 dpl, became predominantly enriched
243 at 6 dpl. In addition to the overall progression from left to right, we noted that cells
244 mapping to reactive MG of the second cluster (cluster 4) and the abutting portion of
245 non-reactive MG (cluster 1) were also enriched at this time point, indicating a reversed
246 direction.

247 Analysis of the cell cycle state further supported our cluster annotation. Specifically,
248 known cell cycle marker genes were used to calculate the predicted cell cycle state
249 (Macosko et al., 2015; Tirosh et al., 2016; Whitfield et al., 2002), and the cell cycle
250 phase (G1, S, G2/M) was projected onto the UMAP of the single cell transcriptome
251 (Figure 2C). Differentiating or differentiated cells were considered as cells in G1 (Wu

252 et al., 2021). Consistently, we observed that most cells of the left side and lower middle
253 part as well as cells branching from the right side of the map were in G1, which
254 comprised most non-reactive MG (clusters 1 and 2), one cluster of reactive MG (cluster
255 4), one RPC population (cluster 7) and the regenerated progeny (clusters 10-15). Cells
256 in S phase were also present on the left side of the map, which represent non-reactive
257 MG (clusters 1 and 2), but were in particular enriched in two domains of the middle
258 part corresponding to reactive MG (cluster 3) and RPCs (clusters 5 and 7). In addition,
259 two domains on the right side of the map showed an accumulation of cells in S phase,
260 which include photoreceptor and horizontal cell precursors (clusters 8 and 9). The
261 pattern of cells in G2/M phase complemented the pattern of cells in G1 and S phase.
262 Cell proliferation pattern was further confirmed by *pcna* expression (Figure 2D). When
263 plotting *pcna* expression onto the main UMAP of the single cell transcriptome, we
264 observed high counts in one population of reactive MG (cluster 3) and in RPCs
265 (clusters 5, 6, 8 and 9). In summary, scRNAseq analysis enabled the establishment of
266 a transcriptome map, which reveals the progressive emergence of non-reactive MG,
267 reactive MG and MG-derived progenitors and regenerated progeny.

268

269 **scRNAseq identifies two populations of non-reactive and two of reactive MG in**
270 **the light-lesioned retina**

271 MG in the homeostatic zebrafish retina are characterized by the expression of GFAP,
272 as well as other canonical glial markers, like *apoeb*, *glula*, *cahz*, *rlbp1a* (Bernardos and
273 Raymond, 2006; Peterson et al., 2001; Raymond et al., 2006; Thummel et al., 2008;
274 Yurco and Cameron, 2005). In our scRNAseq dataset, we found clusters 1 and 2
275 expressing *apoeb*, *glula*, *cahz*, *rlbp1a* as marker genes (Figure 2-figure supplement 2
276 and supplementary file 1). When plotting *apoeb* expression onto the UMAP, we

277 observed high counts in clusters 1 and 2, as well as in clusters 3 and 4 (Figure 3A).
278 The glial marker *gfap*, found among the top 100 upregulated marker genes for cluster
279 4 (supplementary file 1), showed a similar pattern, with high counts in clusters 1 to 4,
280 but displayed high counts in cluster 5 as well (Figure 3A). Given the expression pattern
281 of *apoeb* and *gfap*, we identified clusters 1 to 4 as MG populations. Further analysis
282 indicated clusters 1 and 2 as non-reactive MG and clusters 3 and 4 as reactive MG
283 (Figure 3B, C). Non-reactive MG, which were mostly in G1 and did not express any
284 injury-specific markers (Figure 2-figure supplement 2) showed counts for *mstnb*
285 (Figure 3B). In addition, members of the retinoic acid signalling pathway, like *rdh10a*,
286 *aldh1a3*, *dhrs3a* (D'Aniello et al., 2015; Feng et al., 2010; Holmes and Hempel, 2011)
287 were enriched in these clusters (Figure 3-figure supplement 1A, supplementary file 2).

288 We next looked into differentially expressed genes (DEG) between the non-reactive
289 MG clusters 1 and 2. For instance, the UMAP plot of *inhbaa*, an evolutionarily
290 conserved vertebrate glia marker (Hoang et al., 2020) showed strong expression only
291 in clusters 1, 3 and 4, but not in cluster 2 (Figure 3B, Figure 3-figure supplement 1A,
292 and supplementary file 2). Reactive MG on the other hand downregulated some glial
293 markers, like *glula* and *rlbp1a*, and upregulated inflammatory cytokines, like *crlf1a*,
294 matrix metalloproteases, like *mmp9*, and growth factors like *hbegfa* in the regenerating
295 retina (Figure 2-figure supplement 2, Figure 3-figure supplement 1B, and
296 supplementary file 1). Consistent with that, plotting of *crlf1a* expression onto the UMAP
297 showed high read counts in clusters 3 and 4, as well as in cluster 5 (Figure 3C). Again,
298 DEG analysis showed that reactive MG can be subdivided further, because only cluster
299 3, but not cluster 4 expressed Hairy-related downstream targets of active Notch
300 signalling including *her15.1-1*, *her9* and *her4.1* (Figure 2-figure supplement 2, Figure
301 3-figure supplement 1B, and supplementary file 3). Indeed, the UMAP plot of *her4.1*
302 showed strong expression in cluster 3 as well as in cluster 5 (Figure 3C). To validate

303 the expression of *her4.1* in the regenerating retina we used *in situ* hybridization. In
304 agreement with our scRNAseq dataset, *her4.1* signal was not present in the uninjured
305 retina, but appeared at 44 hpl in the inner nuclear layer of the central retina (Figure
306 3D). At 4 and 6 dpl, *her4.1* transcripts remained in the inner nuclear layer and appeared
307 in cells of the outer nuclear layer too (Figure 3D). We further analysed the expression
308 of *crlf1a*, a marker of reactive MG, with fluorescent *in situ* hybridization combined with
309 immunohistochemistry against GFAP (located mainly to MG fibers) and the
310 proliferation marker PCNA (Figure 4). Consistent with our scRNAseq dataset, *crlf1a*
311 was not detectable in the uninjured, central retina, but was upregulated in Zrf1/PCNA-
312 double positive cells at 44 hpl (Figure 4A, B). At 4 dpl, *crlf1a* signal was still present in
313 Zrf1/PCNA-double positive cells and returned back to undetectable levels at 6 dpl
314 (Figure 4A, B). Taken together, we observed cellular heterogeneity in MG during
315 regeneration, and identified two non-reactive and two reactive MG populations that
316 express distinct marker genes.

317

318 **scRNAseq identifies a transient cell population with hybrid characteristics of**
319 **reactive MG and early RPCs in the light-lesioned retina**

320 As mentioned above, several MG-related genes, like *gfap* or *crlf1a*, were also
321 expressed in cluster 5, which locates next to the reactive MG (clusters 3 and 4), is
322 highly proliferative and only becomes eminent at 4 dpl. Further analysis of this cluster
323 showed expression of several members of the High Mobility Group (Hmg) protein
324 family among the top 100 upregulated marker genes (supplementary file 1). Consistent
325 with that, the UMAP expression profile of *hmgb2b* showed presence of high counts
326 already in cluster 3 (reactive MG), as well as in other, further downstream RPC clusters
327 and regenerating progeny (Figure 5A). This indicated a transition from MG to RPC fate

328 in the course of regeneration and that cells of cluster 5 might have hybrid
329 characteristics of reactive MG and downstream RPCs. Hence, we conducted a DEG
330 analysis of cluster 5 in comparison to reactive MG (clusters 3 and 4), as well as to the
331 neighbouring, downstream RPCs (cluster 6). When compared to reactive MG, cells of
332 cluster 5 showed expression of several genes, including *stmn1a*, *nr2e1* and *sox9b*
333 (Figure 3-figure supplement 1C, supplementary files 4 and 5). Consistently, UMAP
334 expression profile of *stmn1a* showed counts prevalently in cluster 5 and neighbouring,
335 downstream RPCs on the right side of the map, but not in the reactive or non-reactive
336 MG on the left side (Figure 5A). The UMAP profiles of *sox9b* and *nr2e1* showed strong
337 expression almost exclusively restricted to cluster 5. DEG analysis between cluster 5
338 and the neighbouring downstream cluster 6 revealed also expression of *nr2e1* and
339 *sox9b*, but additionally transcripts like *id1* (Figure 3-figure supplement 1D and
340 supplementary file 6). Consistently, high *id1* counts were found in cluster 5 and in other
341 reactive or non-reactive MG clusters, but not in downstream RPCs on the right side of
342 the map (Figure 5A). In order to validate the RNAseq data, we analysed the expression
343 of *hmgb2b* and *id1* transcripts in the regenerating retina using *in situ* hybridization and
344 fluorescent *in situ* hybridization combined with immunohistochemistry, respectively.
345 Consistent with our scRNAseq data, *hmgb2b* signal was not detectable in the
346 uninjured, central retina, but was initiated in individual cells residing in the inner nuclear
347 layer at 44 hpl (Figure 5B). Subsequently, *hmgb2b* transcripts could be detected in
348 clusters of cells in the inner and outer nuclear layers at 4 and 6 dpl (Figure 5B). The
349 expression of *id1* in the regenerating tissue matched the scRNAseq data. Expression
350 of *id1* was already detectable in Zrf1-positive but PCNA-negative cells in the inner
351 nuclear layer of the uninjured, central retina (Figure 6A, B). At 44 hpl, *id1* was strongly
352 upregulated and co-localized with Zrf1/PCNA-double positive cells in the inner nuclear
353 layer. At 4 and 6 dpl, *id1* expression was still associated with Zrf1/PCNA-double

354 positive cells and, occasionally, with PCNA-only positive cells (Figure 6A, B). In
355 summary, marker analysis reveals that cells in cluster 5 display a transcriptional
356 signature of reactive MG, as well as RPCs, which is why we assigned it a hybrid
357 identity.

358

359 **scRNAseq identifies two neurogenic progenitor populations in the light-lesioned**
360 **retina**

361 The before-mentioned DEG-analysis between cluster 5 (hybrid cells) and cluster 6
362 (neighbouring, downstream RPCs) also revealed that the latter upregulated *insm1a*
363 (Figure 3-figure supplement 1D and supplementary file 6), which has been described
364 to promote cell cycle exit of RPCs in the injured fish retina at 4 dpl (Ramachandran et
365 al., 2012). In addition, our DEG analysis showed upregulation of *atoh7* and *onecut2* in
366 cluster 6 (Figure 3-figure supplement 1D and supplementary file 6). We found that the
367 highly redundant gene *onecut1* was also expressed in cluster 6, albeit this was not
368 found in the DEG analysis. As expected, the UMAP expression profile of *insm1a*
369 confirmed high read counts in cluster 6 but also in clusters 7, 8 and 10 (Figure 7A).
370 The UMAP expression profile of *atoh7* also confirmed expression in cluster 6, as well
371 as in clusters 7 and 10 (Figure 7A). Moreover, the UMAP expression profile of *onecut1*
372 and *onecut2* confirmed that both genes were expressed in clusters 6 and 7 and in
373 addition in cluster 9 (Figure 7A). Cluster 7 expressed additional neurogenic marker
374 genes like *tubb5* and *sox11b* (Baraban et al., 2013; Lange et al., 2020; Mu et al., 2016)
375 (Figure 3-figure supplement 1D and supplementary file 1). Finally, the cell cycle status
376 and the UMAP expression of *mki67,* a mitotic marker, showed read counts in cluster
377 6, but not in cluster 7 (Figure 7A). Hence, we concluded that cluster 6 and cluster 7
378 represented neurogenic progenitors, and were named progenitors 2 and progenitors

379 3, respectively. To validate *atoh7*, *onecut1* and *onecut2* expression in the regenerating
380 retina, we employed again *in situ* hybridization. In agreement with our scRNAseq data,
381 *atoh7* signal was absent in the uninjured and 44 hpl retina, but became detectable in
382 the inner and outer nuclear layers at 4 and 6 dpl (Figure 7B). Similarly, *onecut1* and
383 *onecut2* were prominently expressed in the inner and outer nuclear layer at 4 and 6
384 dpl, in addition to their homeostatic expression in the presumptive horizontal cell layer
385 in the uninjured and 44 hpl retina (Figure 7B, black arrowheads). In summary,
386 scRNAseq showed heterogeneity of neurogenic progenitors, which upregulate known
387 markers of retinogenesis in the regenerating retina.

388

389 **scRNAseq identifies fate-restricted progenitors in the light-lesioned retina**

390 Gene expression analysis of cluster 8, which locates next to the neurogenic progenitors
391 (cluster 6 and 7), showed significant upregulation of several well-known photoreceptor
392 precursor markers, including *crx*, and *thrb* (supplementary file 1). Consistently, UMAP
393 plots for *crx* and *thrb* revealed high counts in cluster 8 (Figure 8A). Moreover, the
394 former was also highly expressed in clusters 11 and 12, whereas the latter was
395 restricted to the additional cluster 1. Subsequent further gene expression analysis
396 identified clusters 11 and 12 as differentiating cone photoreceptors arising from cluster
397 8. Precisely, clusters 11 and 12 represent differentiating photoreceptors giving rise to
398 blue and red cones as shown by the UMAP plots of *opn1sw2* and *opn1lw2*, respectively
399 (Figure 8B). Cluster 9, which abuts the neurogenic progenitor 3 (cluster 7), expressed
400 known developmental markers of horizontal cell precursors like *prox1a* and *rem1*
401 (supplementary file 1). Consistently, the UMAP plot for *rem1* showed high expression
402 almost restricted to this cluster specifically. Gene expression analysis also revealed
403 *ptf1a* expression in cluster 9, which has been shown to be required for lineage

404 specification of horizontal and amacrine cells in the developing retina (Jusuf et al.,
405 2011; Jusuf and Harris, 2009). In line with these findings, the UMAP expression profile
406 of *ptf1a* confirms high counts in the left part of cluster 9, but is even more pronounced
407 in the upstream part of cluster 7 feeding into cluster 9 (Figure 8C). Gene expression
408 analysis of the remaining clusters 10, 13, 14 and 15 identified them as differentiating
409 progeny giving rise to retinal ganglion cells (cluster 10), amacrine cells (clusters 13 and
410 14), as well as bipolar cells (cluster 15), respectively (supplementary file 1). In this
411 context, UMAP plots of *gap43* and the more mature retinal ganglion cell marker *isl2b*
412 showed a strong upregulation in cluster 10 (Figure 8D). UMAP plots of *stx1b* and
413 *pvalb6*, markers of differentiating and mature amacrine cells, revealed strong
414 expression in clusters 13 and 14, whereas UMAP plots of *vsx1* and *samsn1a*, known
415 and novel markers of bipolar cells, respectively, showed high counts in cluster 15
416 (Figure 8E, F).

417 With this respect, it was recently shown that the regenerating adult zebrafish retina
418 recapitulates developmental fate specification programs (Lahne et al., 2020a). Hence,
419 we plotted the fraction of cells that differentiate into a specific cell fate during the time
420 course of regeneration (Figure 8-figure supplement 1). We found that the earliest
421 committed progeny emerged at 4 dpl giving rise to retinal ganglion cells or to
422 photoreceptors, in particular red cones. At 6 dpl, the number of retinal ganglion cells
423 and red cones continued to increase. In addition, we detected a significant number of
424 blue cones and amacrine cells, as well as a small number of bipolar cells at this time
425 point. We did not detect any differentiating progeny giving rise to horizontal cells or
426 rods at this stage. To address this issue, we further investigated the expression of more
427 mature neuronal markers in our dataset (Figure 8-figure supplement 2). Expression of
428 *rho* and *gnat1*, two markers of rod photoreceptors, was very low and sparse, and did
429 not define any specific rod cluster (Figure 8-figure supplement 2A). Expression of

430 *gad1b*, which encodes for glutamate decarboxylase synthetizing the neurotransmitter
431 GABA, was mostly restricted to amacrine cells (clusters 13 and 14) (Figure 8-figure
432 supplement 2B). To address the expression of more mature markers of amacrine and
433 horizontal cells, we investigated *chata* (*choline O-acetyltransferase a*, an amacrine
434 cell-specific marker), as well as *calb2a* and *calb2b* (*calbindin 2a* and *calbindin 2b*,
435 markers of amacrine and horizontal cells) (Figure 8-figure supplement 2B, C). As
436 expected, high counts of *chata* were specifically found in amacrine cells (clusters 13
437 and 14). In particular, *chata* expression was detected only in cells located at the tip of
438 cluster 13 and in all cells of cluster 14. *calb2a* was expressed in some reactive MG
439 (cluster 3) and quite strongly in some amacrine cells (cluster 13). Importantly, we did
440 not detect any *calb2a* and *calb2b* in horizontal cell precursors (cluster 9).

441 We also checked the expression of transcripts for variants of protein kinase C using
442 *prkcab* and *prkcbb* (*protein kinase alpha b*, *protein kinase beta b*) to identify mature
443 bipolar cells (Figure 8-figure supplement 2D). Counts for *prkcab* were sparsely found
444 in some non-reactive and reactive MG (clusters 1-4). *prkcbb*-positive cells were found
445 more frequently in some non-reactive and reactive MG (clusters 1-4), progenitor 1
446 (cluster 5), as well as in amacrine cells (clusters 13, 14). Importantly, we did not detect
447 *prkcab* or *prkcbb* in our bipolar cells. When plotting the expression of general synaptic
448 markers like *snap25a* and *snap25b*, we observed mainly transcripts in the
449 differentiating progeny (Figure 8-figure supplement 2E). Specifically, high counts of
450 *snap25a* were found in retinal ganglion and amacrine cells (clusters 10, 13 and 14).
451 High counts of *snap25b* were observed in the same clusters as well as in red and blue
452 cones (clusters 11 and 12) and the right part of the horizontal cell precursors (cluster
453 9). Taken together, our scRNAseq data reveal the presence of fate-restricted
454 progenitors and the sequential appearance of differentiating progeny in the light-
455 lesioned, adult zebrafish retina. Moreover, the analysis of more mature markers shows

456 that the differentiation of retinal ganglion cells and red cones is preceding the
457 appearance of blue cones, amacrine and bipolar cells.

458

459 **DISCUSSION**

460 In this study, we employed a short-term lineage tracing strategy, which allowed the
461 selective enrichment of MG and their respective progeny for up to six days post light
462 lesion. Subsequent scRNAseq resolved the transcriptome of individual MG, RPCs as
463 well as regenerated progeny, and allowed to reconstruct their lineage relationship in
464 the homeostatic and regenerating zebrafish retina (Figure 1). A previous study
465 combined bulk RNA sequencing of sorted MG with scRNAseq of whole retinae from
466 zebrafish upon NMDA as well as light lesions (Hoang et al., 2020). This work focussed
467 specifically on the early reprogramming of MG and progenitor production, covering up
468 to 36 hours post light lesion. The authors report that MG go through an activated, non-
469 proliferative state characterized by upregulation of gliosis markers. However, neither
470 did they find any evidence of MG heterogeneity in uninjured conditions nor did they
471 provide any thorough characterization of MG-derived RPCs (Hoang et al., 2020).
472 Additional RNA sequencing studies of the regenerating zebrafish retina have used
473 microarray as well as RT-PCR and qRT-PCR to evaluate transcriptional changes at a
474 population level, without providing any MG/RPC single cell resolution (Cameron et al.,
475 2005; Craig et al., 2008; Kassen et al., 2007; Kramer et al., 2021; Morris et al., 2011;
476 Ng Chi Kei et al., 2017; Qin et al., 2009). Previous immunohistochemistry and *in situ*
477 hybridization experiments provided a broad description of MG-derived RPCs. Indeed,
478 progenitors are reported as fusiform cells that proliferate and express markers of
479 multipotency like Pax6 and Sox2, as well as some neurogenic markers like Atoh7,
480 Ptf1a, Vsx1 and others (Bernardos et al., 2007; Fausett and Goldman, 2006; Fimbel

481 et al., 2007; Gorsuch et al., 2017; Lahne et al., 2020a; Ramachandran et al., 2012). In
482 contrast to these previous results, our study is the first providing a comprehensive
483 overview of MG, MG-derived cells and their lineage relationship up to 6 days post
484 lesion in the zebrafish retina. Due to our selective enrichment of MG and their
485 respective progeny, we gain an adequate single cell resolution to observe substantial
486 heterogeneity in the molecular identity of MG in homeostatic as well as regenerating
487 conditions. We also provide an in depth description of MG as well as RPC molecular
488 identity, cell fate decisions and production of regenerated progeny that cover all key
489 aspects during zebrafish retina regeneration. Our strategy allowed us to define two
490 main trajectories in the regenerating zebrafish retina (Figure 9). The first trajectory
491 (solid and dashed red lines) comprises clusters 1 to 5 and constitutes a closed cycle
492 that both maintains the MG pool and generates the first-born neurogenic RPCs. The
493 second trajectory (solid black lines) involves clusters 6 to 15 and gives rise to all retinal
494 neurons via the progressive restriction in cell fate competence of neurogenic RPCs.
495 We discuss the two trajectories separately.

496

497 **Müller glia self-renew and give rise to early, multipotent progenitors**

498 The glial trajectory starts with non-reactive MG (clusters 1 and 2), which express
499 canonical glial markers like *gfap*, *apoeb* and additional genes like *glula*, *rlbp1a* and
500 *cahz* that ensure the housekeeping function of MG during homeostasis (Figure 3A,
501 Figure 2-figure supplement 2, supplementary file 1). Most cells in the non-reactive MG
502 clusters are quiescent based on the analysis of the cell cycle, and are frequently found
503 in the uninjured, but also in the lesioned retina at all sampled time points (Figure 2).
504 However, some non-reactive MG are in S or G2/M phases of the cell cycle, and
505 express *pcna*, albeit at a lower level as compared to the expression in injury-induced,

506 proliferating cell clusters (Figure 2C, D). This is consistent with the proposed model
507 that zebrafish MG proliferate occasionally also in the uninjured, central retina and
508 generate rod progenitors that feed the rod precursor pool at the base of the outer
509 nuclear layer (Bernardos et al., 2007; Stenkamp, 2007). Accordingly, we detect PCNA-
510 positive cells in the uninjured, central retina (Figure 1-figure supplement 1) as well as
511 a small fraction of cells that align in a trajectory from non-reactive MG on the left
512 through reactive MG in the middle, to photoreceptor precursors on the right side of the
513 UMAP in the uninjured retina (Figure 2B). However, some cells end up in the amacrine
514 as well as retinal ganglion cell clusters. This suggests that MG might have the potential
515 to generate not only rods, but also all other retinal neurons in the homeostatic adult
516 retina. Indeed, MG in the uninjured retina express, albeit at a low level, multipotency
517 markers like *pax6*, and share many marker genes with RPCs (Bernardos et al., 2007;
518 Blackshaw et al., 2004; Raymond et al., 2006). Still, MG and injury-induced RPCs are
519 considered distinct cell populations. Upon injury, MG divide only once between 31 and
520 48 hpl, whereas MG-derived RPCs continue to divide, reaching a peak of proliferation
521 at 4-5 dpl (discussed in Fausett and Goldman, 2006; Lahne et al., 2020a; Lenkowski
522 and Raymond, 2014; Thummel et al., 2008). We isolated cells at 44 hpl, a time point
523 when MG are about to undergo, or already underwent, their asymmetric cell division
524 (Bernardos et al., 2007; Lahne et al., 2015; Lenkowski and Raymond, 2014;
525 Nagashima et al., 2013) and identify cells in cluster 3 as early reactive MG. Consistent
526 with that, we find that cells in cluster 3 do not only express *gfap* and *apoeb*, but also
527 *pcna* (Figure 2D, 3A). Moreover, the predicted cell cycle status supports this notion.
528 Whereas cells in the left part of cluster 3 are mostly in G1, cells in G2/M phase are
529 found in the right part, with cells in S phase overlapping with both domains (Figure 2C).
530 Cells in cluster 3 also upregulate inflammation-related markers like *crlf1a*, as well as
531 *mmp9* and *hbegfa* (Figure 3C, 4, Figure 3-figure supplement 1B and supplementary

532 file 1). The upregulation of inflammatory genes makes MG similar to immune cells
533 (Silva et al., 2020; Wan et al., 2012; Zhao et al., 2014). In this context, our population
534 of early reactive MG (cluster 3), identified mostly at 44 hpl, resembles the reactive MG
535 pool found in the regenerating zebrafish retina at 36 hpl (Hoang et al., 2020). However,
536 our MG cluster is proliferative, whereas the one discussed by the mentioned study is
537 not. The presence of a distinct pool of non-proliferative, reactive MG as early as 36 hpl
538 in the earlier study might be explained by the different time points of sample collection,
539 and/or by the lower number of cells sequenced in our experiment (11.690) in
540 comparison to the previous one (45.153) (Hoang et al., 2020). In summary, MG in the
541 homeostatic zebrafish retina behave like multipotent RPCs. Upon injury, reactive MG
542 express genes associated with inflammation, like *crlf1a*, and undergo asymmetric cell
543 division. Daughter cells derived from this cell division most likely map to cluster 5,
544 which is discussed below.

545

546 **A crossroad in the glial trajectory: hybrid cells with MG and RPC characteristics**

547 The close similarity between zebrafish MG and MG-derived RPCs at the level of
548 expressed markers as well as cellular and subcellular morphology has been described
549 extensively in the literature (Fausett and Goldman, 2006; Lahne et al., 2020b;
550 Lenkowski and Raymond, 2014). Thus, we suggest that cells in cluster 5, which
551 displays a transcriptional hybrid identity between MG and RPCs, are the product of the
552 asymmetric cell division from the early reactive MG (cluster 3). Cells in cluster 5 are
553 still *gfap* positive, and share marker expression with early reactive MG, like *her4.1* and
554 *crlf1a* (Figure 3A, C). However, cluster 5 is highly proliferative and becomes only
555 prominent at 4 dpl, a time point when predominantly RPCs are proliferating (Bernardos
556 et al., 2007; Fausett and Goldman, 2006; Lenkowski and Raymond, 2014; Nagashima

557 et al., 2013). Consistently, *pcna* is highly expressed in cluster 5 and the predicted cell
558 cycle status indicates that most cells are in S or G2/M phase (Figure 2C, D). Moreover,
559 previous studies have found *her4.1* and *crlf1a* in MG-derived RPCs in the light- as well
560 as stab-lesioned retina, where they control RPC proliferation at 4 dpl (Wan et al., 2012;
561 Wilson et al., 2016; Zhao et al., 2014). We found that *her4.1* at 4 and 6 dpl locates to
562 the inner nuclear layer as well as to the outer nuclear layer, where presumptive RPCs
563 reside at this time point (Figure 3D) (Campbell et al., 2022; Wilson et al., 2016). In
564 addition, cells in cluster 5 upregulate *sox9b* and *nr2e1*, which have been found in early,
565 multipotent RPCs of the developing fish, avian and mammalian retinae, as well as in
566 late retinogenesis, where they regulate MG genesis (Buenaventura et al., 2018; Corso-
567 Díaz and Simpson, 2015; Kitambi and Hauptmann, 2007; Muto et al., 2009; Poché et
568 al., 2008). Hence, we propose that cells in cluster 5 represent a crossroad of the glial
569 and neurogenic trajectory, containing self-renewed MG as well as first-born, MG-
570 derived RPCs as a direct result of the earlier (44 hpl) asymmetric MG cell division. We
571 further propose that self-renewed MG close the cycle via late reactive MG (cluster 4)
572 and return into non-reactive MG (clusters 1 and 2, red, dashed line in Figure 9). In
573 contrast, MG-derived RPCs embark into the neurogenic pathway (cluster 6, solid, black
574 line). In an alternative model, cells in cluster 5 might represent only MG cells that have
575 upregulated early RPC markers like *sox9b* and *nr2e1* and are dividing a second time
576 at 4 dpl to generate renewed MG (cluster 4) and neurogenic RPCs (cluster 6).
577 However, MG have been described to divide only once between 31 and 42 hpl and
578 additional and/or asynchronous MG divisions later than 2 dpl have not been
579 investigated (Lahne et al., 2015; Lenkowski and Raymond, 2014; Nagashima et al.,
580 2013). BrdU/EdU lineage tracing experiments will be required to address this issue,
581 with the caveat that MG and RPCs are hardly distinguishable from each other in the 4
582 dpl retina, especially when using the Zrf1 antibody to label MG (Fausett and Goldman,

583 2006; Raymond et al., 2006). Live imaging of the regenerating retina would be the best
584 tool to follow MG and MG-derived progenitors *in vivo*, but the technique is not optimized
585 yet for long recordings from the intact tissue in the living animal (Lahne et al., 2015).
586 Either way, our proposed model of self-renewing MG is further supported by the
587 change of cell density over time (Figure 2B). Following the cells across the four time
588 points on the UMAP, we observe that initially most cells of the uninjured sample map
589 to non-reactive MG (clusters 1 and 2) located at the far left. At 44 hpl, the cell density
590 shifts towards the upper right portion of cluster 1 and towards the early reactive MG
591 (cluster 3) in the upper, middle of the map. At 4 dpl, sampled cells mostly map to RPCs
592 (clusters 5-9) on the right, as well as to late reactive MG (cluster 4) in the lower, middle
593 part. Additionally, cells mapping to the lower right part of non-reactive MG (clusters 1
594 and 2) are enriched in this sample, indicating a reverse direction from right to left. This
595 population is significantly further increased at 6 dpl, when the number of RPCs is less
596 prominent and the differentiating neural types at the top and bottom right are
597 predominantly present in the sample. According to this model, sample collection at
598 even later time points, e.g. 10 or 14 dpl, might show that the initial status has been
599 restored and that non-reactive MG are mostly enriched. However, it is unlikely that this
600 experiment could be performed with our short-term labelling strategy.

601

602 **The neurogenic trajectory produces regenerated progeny that partially follow**
603 **the developmental order of neurogenesis**

604 Neurogenic RPCs map to the right of cluster 5, and include proliferating, neurogenic
605 RPCs (cluster 6) and the downstream, non-proliferating, neurogenic RPCs (cluster 7).
606 Cells in these clusters express *insm1a*, *atoh7* and additional neurogenic genes that
607 are required for the generation of several neuronal lineages (Figure 7, Figure 3-figure

608 supplement 1D and supplementary files 1 and 6). Indeed, *atoh7* expression has been
609 described to be initiated in RPCs on their way to the last cell division giving rise to a
610 retinal ganglion cell and another cell that can be either an amacrine cell, or a precursor
611 of a horizontal or of a cone cell in the developing zebrafish retina (Amini et al., 2018;
612 Nerli et al., 2022; Poggi et al., 2005). Cluster 6 and 7 appear also highly similar to the
613 transient, neurogenic RPC state that has been described recently in the developing
614 mouse retina (Wu et al., 2021). We propose that cluster 6 and 7 are the roots of the
615 neurogenic trajectory from which fate-restricted RPCs and regenerated progeny arise
616 at 4 and 6 dpl (solid, black line in Figure 9). Cells in cluster 6 are *mki67*-positive, but
617 additionally express *insm1a*, which promotes RPC cell cycle exit at 4 dpl in the injured
618 retina (Ramachandran et al., 2012). Cells in cluster 6 might undergo their last cell
619 division, as suggested by the concomitant expression of *atoh7*. Consistently, in our
620 scRNAseq high counts of *atoh7* are found in cells of cluster 6, to cluster 7 and
621 eventually cluster 10. Cluster 10 represents differentiating retinal ganglion cells that
622 are the first regenerated progeny, evident as early as 4 dpl (Figure 7, 9 and Figure 8-
623 figure supplement 1).

624 While amacrine cells arise directly from the core of neurogenic RPCs, fate restricted
625 precursors for regenerated cones and for horizontal cells are identified (Figure 8 and
626 9), as it occurs during development (Godinho et al., 2007; Weber et al., 2014).
627 Consistently with the events during development, red cones (cluster 11) branch from
628 *thrb*-positive cells of the photoreceptor RPC cluster (cluster 8). Interestingly, *thrb*
629 transcripts are found in neurogenic RPCs of cluster 7 as well as at the beginning of
630 cluster 9, which contains horizontal cell precursors becoming evident at 4 dpl (Figure
631 8B). This is in agreement with observations in the developing zebrafish retina, where
632 horizontal and cone cells share a common Thrb-positive progenitor (Suzuki et al.,
633 2013). Mature markers of horizontal cells, like calbindins, are not found in cluster 9

634 (Figure 8B, Figure 8-figure supplement 2C and supplementary file 1), in contrast to
635 cone photoreceptor mature markers, like opsins, at 4 and 6 dpl. While it might be that
636 mature horizontal cells arise later than 6 dpl, their absence from our dataset could also
637 be due to our experimental set-up. As explained before, we isolated mCherry-only
638 positive and EGFP/mCherry-double positive cells to obtain MG and MG-derived cells.
639 Whereas mCherry, driven by a *gfap* promoter fragment, is actively transcribed in MG,
640 the label of MG-derived cells is completely dependent on the half-life of the fluorophore.
641 Protein turnover and further cell divisions would result in a constant depletion of
642 mCherry in MG-derived cells over time. In this context, we find a strong expression of
643 *pcna* in cluster 9, indicating that additional cell divisions might have diluted the mCherry
644 label to undetectable levels (Figure 2D). Inclusion of EGFP-positive only cells in our
645 sample collection may reveal the pool of mature horizontal cells, which inherit the
646 fluorophore from their *pcna:EGFP*-positive precursors. Accordingly, we find the
647 presence of horizontal cell precursor markers in our dataset. For instance, cells in
648 cluster 9 express *onecut1* and *onecut2*, which encode transcription factors and are
649 upregulated in horizontal cell RPCs in the developing mouse retina, and which regulate
650 horizontal cell maintenance in adult animals (Emerson et al., 2013; Klimova et al.,
651 2015; Sapkota et al., 2014). Counts for *onecut1* and *onecut2* are found also in earlier
652 neurogenic RPCs of clusters 6 and 7, where they most likely contribute to the transient
653 state of RPCs together with additional neurogenic markers, like *atoh7* (Wu et al., 2021).
654 This is again consistent with observations in the developing mouse retina, where
655 Onecut1 and Onecut2 regulate the development of retinal ganglion cells, as well as
656 the development of cones, horizontal cells, and of a subset of amacrine cells, while
657 inhibiting rod specification genes (Emerson et al., 2013; Sapkota et al., 2014).

658 In addition to mature horizontal cells, we were also unable to detect any rod-specific
659 cluster expressing mature rod markers like *rho* and *gnat1* (Figure 8-figure supplement

660 2A). We assume that mature rods might arise as a third branch from the photoreceptor
661 RPC cluster (Figure 9), which indeed expresses rod specification markers like *nr2e3*
662 (supplementary file 1). We speculate that rods either become evident only later than 6
663 dpl, or that they do not survive the isolation procedure, since rods possess a complex
664 morphology with long outer segments. A third possibility might be that rod
665 photoreceptors are replenished by their dedicated rod precursors faster than the
666 triggering of the MG-dependent injury response. In this context, rod precursors form a
667 pool of cells at the base of the outer nuclear layer and proliferate as early as 16 hours
668 post-light lesion (Morris et al., 2005; Stenkamp, 2011; Thummel et al., 2008). Since
669 the already available pool of rod precursors would be *gfap*:mCherry-negative, we might
670 have missed the derived rod progeny, given our sorting strategy. In summary, we show
671 that in the light-lesioned retina, zebrafish MG go through an inflammatory-like state
672 before generating hybrid MG/RPCs that eventually cycle-back to non-reactive MG as
673 well generate neurogenic RPCs. The neurogenic RPCs progressively restrict their
674 competence to produce neurons that include retinal ganglion cells first and bipolar cell
675 last up to 6 dpl. Our study is the first comprehensive description of the molecular
676 network underlying MG self-renewal and RPC differentiation to regenerating neurons
677 which will inform future regenerative therapies to treat retinal dystrophies in
678 humans.(Javed and Cayouette, 2017).

679

680 **MATERIALS AND METHODS**

681 **Animals**

682 Zebrafish (*Danio rerio*) were raised as previously described (Brand et al., 2002). Adult
683 fish (6-12 months old) of either sex were used for all experiments. WT animals were in
684 the AB genetic background.

685

686 **Transgenic lines**

687 To generate the *Tg(pcna:EGFP)* (tud119), the BAC CH73-140L11, containing more
688 than 100 kb of the genomic *pcna* locus, was obtained from the BACPAC resource
689 centre. A cassette containing EGFP and a polyadenylation signal was recombined at
690 the starting ATG of exon 1. First, FRTgb- neo-FRT and EGFP cassettes where
691 amplified by PCR. Then, the cassettes where amplified and merged by fusion PCR
692 with primers carrying 50 nucleotides of homology of the targeting sequence.
693 Recombineering of the BAC was performed as previously described (Zhang et al.,
694 1998). BAC DNA was purified and about 50 pg of BAC DNA were injected into fertilized
695 eggs at the one cell stage. F0 were raised and incrossed. F1 were identified by visual
696 screening for GFP expression and raised. The *Tg(gfap:nls-mCherry)* line was
697 generated as previously described (Lange et al., 2020). In addition, to the line
698 described in Lange et al. (tud117tg), a second independent insertion was isolated
699 (tud120). This insertion displays a stronger expression in MG and was hence used for
700 this study.

701

702 **Light injury**

703 WT AB and *Tg(pcna:EGFP);Tg(gfap:nls-mCherry)* fish were dark adapted for 3 days.
704 Afterwards, diffuse light lesion was performed as previously described (Weber et al.,
705 2013). Briefly, up to 4 fish were placed in a beaker filled with system water (300 ml),
706 positioned 3 cm away from the light bulb of a metal halide lamp (EXFO X-Cite 120W,
707 EXFO Photonic Solutions, Mississauga, Ontario, Canada). Fish were exposed for 30
708 min to a bright light (≥ 100.000 lux), and then put back to system tanks in normal light

709 conditions. Uninjured fish controls were dark adapted and processed in parallel to light
710 injured animals.

711

712 **Dissociation of retinae to a single cell suspension**

713 Uninjured and light-lesioned *Tg(pcna:EGFP);Tg(gfap:nls-mCherry)* fish were exposed
714 to an overdose (0.2%) of MS-222 (Sigma) (Brand et al., 2002) until cessation of the
715 operculum movement. Subsequently, each cornea was poked with a needle, and
716 tweezers were gently pressured on each side of the eye to remove the lens. Then,
717 tweezers were used to carefully isolate the retinae, which were put in a dissociation
718 solution of papain (16 U/ml), dispase (0.2 U/ml) and DNAse (168 U/ml) dissolved in
719 Earle's Balanced Salt Solution (EBSS, Worthington Biochemical Corporation). Up to 6
720 retinae were put in 1.7 ml of dissociation solution. Retinae were digested for 30 minutes
721 at 28°C, and then calcein blue (final concentration: 1μM, Invitrogen) was added for 10
722 minutes to the digestion solution at 28°C to stain for living cells. At the end of the
723 enzymatic digestion, mechanical trituration was applied using fire-polished glass
724 pipettes of decreasing tip diameter to help tissue dissociation. Single cells were
725 centrifuged (300 g) at 4°C, for 6 minutes. The cell pellet was re-suspended in EBSS
726 supplemented with DNAse (100 U/ml) to eliminate residual, ambient DNA, and albumin
727 ovomucoid inhibitor (1:10 of stock solution, Worthington Biochemical Corporation) to
728 stop papain action. The single cell solution was eventually filtered (20 μm filters) to
729 remove clumps and debris, and put on ice, ready for Fluorescent Activated Cell Sorting
730 (FACS). Each single cell suspension was obtained by pooling 8 retinae (from 4 fish, 2
731 males and 2 females) of uninjured and light-lesioned
732 *Tg(pcna:EGFP);Tg(gfap:mCherry)* animals. Uninjured WT AB, *Tg(gfap:mCherry)* and
733 *Tg(pcna:EGFP)* fish were used to prepare single cell suspensions of dissected retinae

734 for setting the single fluorophore gates in flow cytometry. Additionally, a calcein only
735 stained single cell suspension was prepared from uninjured WT AB fish retinae for the
736 setting of the calcein gate in the flow cytometry.

737

738 **Flow cytometry and FACS**

739 A BD FACSAria™ III cell sorter was used for flow cytometry and FACS. mCherry
740 fluorophore was detected using a 561 nm excitation laser and a 610/20 nm band pass
741 filter, EGFP using a 488 nm laser and a 530/30 nm band pass filter and calcein blue
742 using a 405 nm laser and a 450/40 nm band pass filter. The gating strategy is shown
743 in Figure 1-supplemental figure 3 for uninjured samples and was the same for all the
744 light-lesioned samples. Forward and side scatters were used to gate cells among all
745 the events in the single cell suspension and to gate singlets among those cells (Figure
746 1-figure supplement 3A). mCherry-positive only as well as EGFP-positive only gates
747 were set in comparison to the unstained, WT control (Figure1-figure supplement 3B).
748 Calcein blue positive, single cells were eventually gated as living cells (60.000 living
749 cells from uninjured, 44 hpl and 4 dpl samples, 41.389 living cells from 6 dpl sample).
750 15.000 cells were sorted from each samples, put on ice and sent to the CMCB Deep
751 Sequencing Facility for single cell RNA sequencing (scRNAseq).

752

753 **(Droplet based) single cell transcriptomics**

754 Single cell transcriptome sequencing was performed based on the 10x Genomics
755 Single cell transcriptome workflow (Zheng et al., 2017). Specifically, 15.000 FACS-
756 sorted cells were recovered in BSA-coated tubes containing 5 ul PBS with 0.04% BSA.
757 Cell samples were carefully mixed with Reverse Transcription Reagent (Chromium

758 Single Cell 3' Library Kit v3) and loaded onto a Chromium Single Cell B Chip to reach
759 a recovery of 10.000 cells per sample. The samples were processed further following
760 the guidelines of the 10x Genomics user manual for single cell 3' RNA-seq v3. In short,
761 the droplets were directly subjected to reverse transcription, the emulsion was broken
762 and cDNA was purified using silane beads (Chromium Single Cell 3' Gel Bead Kit v2).
763 After amplification of cDNA with 11 cycles, samples were purified with 0.6x volume of
764 SPRI select beads to deplete DNA fragments smaller than 400 base pairs and cDNA
765 quality was monitored using the Agilent FragmentAnalyzer 5200 (NGS Fragment Kit).
766 10 ul of the resulting cDNA were used to prepare single cell RNA seq libraries -
767 involving fragmentation, dA-Tailing, adapter ligation and 11 cycles of indexing PCR
768 following manufacturer's guidelines. After quantification, both libraries were sequenced
769 on an Illumina NextSeq500 in 75 base pair paired-end mode, generating 45-109 million
770 fragments per transcriptome library. The raw sequencing data was processed with the
771 'count' command of the Cell Ranger software (v2.1.0) provided by 10X Genomics. To
772 build the reference, the zebrafish genome (GRCz11) as well as gene annotation
773 (Ensembl 90) were downloaded from Ensembl and the annotation was filtered with the
774 'mkgtf' command of Cell Ranger (options: '—e attribute=gene_biotype:protein_coding
775 --attribute=gene_biotype:lincRNA –attribute=gene_biotype:antisense'). Genome
776 sequence and filtered annotation were then used as input to the 'mkref' command of
777 Cell Ranger to build the appropriate Cell Ranger.

778

779 **Bioinformatic analysis**

780 The complete software stack for the analysis is available as a Singularity container
781 (https://gitlab.hrz.tu-chemnitz.de/dcgc-bfx/singularity/singularity-single-cell, tag
782 1f5da0b). The count matrices generated with Cell Ranger were further analysed using

783 scanpy 1.8.2 (https://genomebiology.biomedcentral.com/articles/10.1186/s13059-
784 017-1382-0). For quality control, we removed cells with less than 2.000 counts, less
785 than 500 detected genes, more than 15% mitochondrial reads or more than 60% of the
786 counts in the top 50 highest expressed genes. The counts were normalised with the
787 size factors computed with calculateSumFactors from scran 1.18.5
788 (min.mean=0.1)(Lun et al., 2016). The normalised counts were log-transformed using
789 the numpy function log1p. The top 4000 highly variable genes were detected using the
790 scanpy function scanpy.pp.highly_variable_genes (n_top_genes= 4000). Cell cycle
791 scores were computed using scanpy.tl.score_genes_cell_cycle on each sample
792 separately. As genes associated to S-phase, the genes *mcm5*, *pcna*, *tyms*, *fen1*,
793 *mcm2*, *mcm4*, *rrm1*, *unga*, *gins2*, *mcm6*, *cdca7a*, *dtl*, *prim1*, *uhrf1*, *si:dkey-185e18.7*,
794 *hells*, *rfc2*, *rpa2*, *nasp*, *rad51ap1*, *gmnn*, *wdr76*, *slbp*, *ccne2*, *ubr7*, *pold3*, *msh2*, *atad2*,
795 *rad51*, *rrm2*, *cdc45*, *cdc6*, *exo1*, *tipin*, *dscc1*, *blm*, *casp8ap2*, *usp1*, *pola1*, *chaf1b*, *brip1*
796 and *e2f8* were used. As genes associated to G2/M phase, the genes *hmgb2a*, *cdk1*,
797 *nusap1*, *ube2c*, *birc5a*, *tpx2*, *top2a*, *ndc80*, *cks2*, *nuf2*, *cks1b*, *mki67*, *tmpoa*, *cenpf*,
798 *tacc3*, *smc4*, *ccnb2*, *ckap2l*, *aurkb*, *bub1*, *kif11*, *anp32e*, *tubb4b*, *gtse1*, *kif20ba*,
799 *si:ch211-69g19.2*, *jpt1a*, *cdc20*, *ttk*, *kif2c*, *rangap1a*, *ncapd2*, *dlgap5*, *si:ch211-*
800 *244o22.2*, *cdca8*, *ect2*, *kif23*, *hmmr*, *aurka*, *anln*, *lbr*, *ckap5*, *cenpe*, *ctcf*, *nek2*, *g2e3*,
801 *gas2l3*, *cbx5* and *selenoh* were used. A principal component analysis (PCA) was
802 performed on the highly variable genes (function scanpy.pp.pca using
803 svd_solver='arpack'). A k-nearest-neighbour (knn) graph was computed using
804 scanpy.pp.neighbors and a UMAP was computed using scanpy.tl.umap. Clustering
805 was performed with scnapy.tl.leiden (resolution= 0.01). For the three resulting clusters,
806 marker genes were computed using scanpy.tl.rank_genes_groups. Two smaller
807 clusters identified as microglia and low-quality cells were removed from the
808 downstream analysis. Detection of highly variable genes PCA were performed as

809 above on the remaining cells. A new knn graph was computed (this time with
810 n_neighbors= 50) and a new UMAP was computed. Embedding densities were
811 computed using scanpy.tl.embedding_density. Clustering was performed in multiple
812 steps, always using scanpy.tl.leiden: First, the data were clustered with the resolution
813 parameter set to 0.45. Next, cluster 10 was subclustered with resolution 0.1 and cluster
814 0 was subclustered with resolution 0.2. Marker genes of the resulting 15 clusters were
815 computed with scanpy.tl.rank_genes_groups. Differential expression analysis of pairs
816 of clusters was performed by subsetting the data to cells from those two clusters and
817 computing differentially expressed genes with scanpy.tl.rank_genes_groups. The
818 source code for the analysis is available on GitHub
819 (https://github.com/fbnrst/celotto_2023).

820 **Cluster annotation**

821 Cluster annotation was performed in several steps. Initially, we identified clusters by
822 considering the top 100 upregulated genes per cluster, the time point at which they
823 appeared and their cell cycle profile. Genes were manually annotated by consulting
824 the ZFIN database (http://zfin.org/) and Pubmed (https://pubmed.ncbi.nlm.nih.gov/)
825 indexed literature about retina development and regeneration. In particular, we took as
826 a reference the single cell RNA sequencing dataset of the regenerating zebrafish retina
827 from Hoang et al., 2020, for marker genes lists. Following the initial identification of cell
828 clusters, we proceeded with a finer characterization by considering differential gene
829 expression analysis for clusters that shared a similar identity. Occasionally (e.g., in the
830 case of horizontal cell precursor marker *ptf1a*), we plotted the UMAP profile of known
831 candidates from retina development or regeneration. Selected marker genes were then
832 checked for expression in the retina tissue via *in situ* hybridization, fluorescent *in situ*
833 hybridization and immunohistochemistry on cryosections.

834

835 **Tissue preparation and cutting**

836 Fish heads were fixed with 4% paraformaldehyde in 0.1 M phosphate buffer (PB, pH:
837 7.4) overnight, at 4°C. Subsequently, fixed heads where decalcified and cryoprotected
838 in 20% EDTA and 20% sucrose in 0.1M PB (pH: 7.5) overnight, at 4°C. Heads were
839 eventually embedded in 7.5% gelatin, 20% sucrose in 0.1M PB and sectioned (12 or
840 14 µm) at the cryostat (CryoStar Nx70, Thermo Scientific). Cryosections were stored
841 at -20°C.

842

843 ***in situ* hybridization probe synthesis**

844 For the synthesis of *in situ* hybridization RNA probes, 4 dpl retinae were dissected and
845 sonicated at 4°C to homogenate the tissue and to extract total RNA. We chose 4 dpl
846 samples, because transcripts of interest were enriched at 4 dpl. RNA was extracted
847 using the total RNA purification kit and following manufacturer's instructions (Norgen
848 Biotek Corporation). cDNA was then transcribed using the first strand cDNA synthesis
849 kit (Roche), followed by PCR to amplify the fragments of interest using primer pairs
850 listed in the key resource table. The amplicon was subsequently purified (gel and DNA
851 recovery kit, Zymo Research) and cloned in a TOPO TA® vector (Thermo Fisher), with
852 which competent *E coli* bacteria were transformed and cultured on Petri dishes coated
853 with agar and ampicillin, overnight at 37°C. The next day, colonies were picked up and
854 cultured in LB medium supplemented with ampicillin (1:2000) overnight at 37°C,
855 shaking, to enrich cultures for mini-prep (Gene Jet Plasmid Miniprep kit k0503, Thermo
856 Fisher). Purified plasmids were sent for sequencing (Eurofins) to verify the sequence.
857 Insert-positive colonies were further enriched in LB/ampicillin cultures for midi-prep

858 (Nucleo Bond® Xtra Midi, Macherey – Nagel) and purified plasmids were linearized to
859 transcribe anti-sense, digoxigenin labelled (DIG) RNA probes, which were stored in
860 hybridization buffer at -20°C. Probes for *her4.1*, *crlf1a*, *hmgb2b*, *onecut1*, *onecut2* were
861 transcribed from a TOPO TA® cloned insert. Instead, the *id1* probe was transcribed
862 directly from the PCR – amplified cDNA using SP6-conjugated forward and T7-
863 conjugated reverse primers (key resource table).

864

865 ***in situ* hybridization**

866 *in situ* hybridization and fluorescent i*n situ* hybridization were performed on three
867 animals per injured time point and on three uninjured controls processed in parallel.
868 Cryosections were dried for 30 minutes at room temperature, then washed two times
869 for 10 minutes in phosphate buffer saline supplemented with 0.3% Triton X-100
870 (PBSTx) for permeabilization. *in situ* hybridization probes were denatured by warming
871 up at 70°C for 10 minutes and brief vortexing. Permeabilized sections were incubated
872 overnight in denatured probes at 62°C. The next day, sections were rinsed three times
873 (once for 15 minutes, followed by two washes of 30 minutes each) in washing buffer
874 (refer to key resource table) at 62°C. Then, in the case of chromogenic *in situ*
875 hybridization, sections were washed twice in MABT (key resource table) for 30 minutes
876 each and incubated with 2% digoxigenin blocking reagent (key resource table) in
877 MABT for 1 hour at room temperature. In the case of fluorescent *in situ* hybridization,
878 sections were washed in TNT buffer (key resource table), and then incubated with 2%
879 digoxigenin blocking reagent dissolved in TNT buffer. After, sections were incubated
880 with the AP-conjugated, anti-digoxigenin antibody (chromogenic *in situ* hybridization,
881 1:2000, key resource table) or with the POD-conjugated, anti-digoxigenin antibody
882 (fluorescent *in situ* hybridization, 1:2000, key resource table) overnight, at 4°C. The

883 next day, sections were washed four times for 20 minutes each in MABT (chromogenic
884 *in situ* hybridization) or three times for 10 minutes each in TNT buffer (fluorescent *in*
885 *situ* hybridization) at room temperature. Then, sections for chromogenic *in situ*
886 hybridization were washed for 5 minutes in staining buffer (key resource table) and
887 eventually incubated with 20 µl/ml NBT/BCIP stock solution in staining buffer, at room
888 temperature, to develop the colour reaction. Time of incubation varied between three
889 hours and overnight, depending on the target mRNA and probe concentration. In the
890 case of fluorescent *in situ* hybridization, after TNT washing steps, sections were
891 incubated for 30 minutes with 1:200 Cy3-Tyramide in TSA amplification buffer (Akoya
892 Biosciences®), at room temperature. Finally, sections from chromogenic *in situ*
893 hybridization were washed three times with PBS, for 10 minutes each and mounted in
894 70% glycerol in PBS, ready for bright field microscopy. Fluorescent *in situ* hybridization
895 sections were rinsed three times in PBS, for 10 minutes each, and then incubation with
896 primary antibody for immunohistochemistry was performed as described below.

897

898 **Immunohistochemistry**

899 Immunohistochemistry was conducted as previously described (Grandel et al., 2006;
900 Kroehne et al., 2011). Immunohistochemistry was performed on three light-lesioned
901 animals and three, parallel processed, uninjured control per condition. Sections were
902 dried at room temperature for 30 minutes and washed 3 times in PBSTx for 10 minutes
903 each. Then, primary antibodies diluted in PBSTx were applied overnight at 4°C (refer
904 to the key resource table for primary antibody host, antigen specificity and dilution).
905 For proliferating cell nuclear antigen (PCNA) retrieval, sections were immersed in 10
906 mM sodium citrate (pH: 6) for 6 minutes at a temperature higher than 80°C, then
907 washed, and finally primary anti-PCNA antibody was applied. After primary antibody

908 incubation, sections were washed three times in PBSTx for 10 minutes each, then
909 Alexa® fluorophore conjugated, secondary antibodies diluted In PBSTx were applied
910 accordingly (refer to key resource table for secondary antibody host, primary antibody
911 specificity and dilution) for 2 hours at room temperature. Sections were eventually
912 washed three times in PBS, mounted in 70% glycerol in PBS, and stored at 4°C. Each
913 staining was performed on three fish per time point upon injury and on three uninjured
914 fish controls processed in parallel. When combined with fluorescent *in situ*
915 hybridization, immunohistochemistry followed fluorescent *in situ* hybridization
916 processed sections.

917

918 **Microscopy**

919 Bright field images of chromogenic *in situ* hybridizations and fluorescent images in
920 Fiure1-figure supplement 2 were acquired with the Widefield ApoTome microscope
921 (Zeiss Axio Imager.Z1) using the 20x/0.8 Plan-Apochromat, Air, DIC objective.
922 Fluorescent images in Figure1-figure supplement 1, and in Figure 4 and 6 were
923 acquired with the laser scanning confocal microscope 780 (Zeiss Axio Imager.Z1)
924 using the 40x/1.2 C-Apochromat, Water, DIC, Zeiss (Figure1-figure supplement 1 and
925 Figure 4) and the 20x/0.8 Plan-Apochromat, Air, DIC, Zeiss (Figure 6). Fluorescent
926 channels were acquired sequentially to minimize crosstalk in multicolour specimens.

927

928 **Image acquisition and processing**

929 Bright field microscope images were processed with the Zeiss ZEN blue, V 2012
930 software. The extended depth of focus function (contrast method) was applied to raw,
931 bright field images of *her4.1*, *hmgb2b*, *atoh7* and *onecut1 in situ* hybridizations to

932 project the chromogenic signal of the optical stack to a single plane. Fluorescent
933 microscope images were processed using Fiji (Schindelin et al., 2012) for image
934 contrast adjustments, crop and rotation. Adobe Illustrator CC 2015.3 was used to
935 assemble figures. Excel 2016 (Microsoft) was used to generate the plot in Figure 8-
936 figure supplement 1.

937

938 **STATISTICS**

939 Marker genes were ranked by their test statistic computed with a t-test for each gene,
940 comparing cells within the cluster to the cells outside the cluster, as implemented in
941 the scanpy function tl.rank_genes_groups. The same was done to identify differentially
942 expressed genes between pairs of clusters.

943

944 **ETHICAL STATEMENT**

945 Fish were kept according to FELASA guidelines (Aleström et al., 2020; Brand et al.,
946 2002). All animal experiments were conducted according to the guidelines and under
947 supervision of the Regierungspräsidium Dresden (permit: TVV 44/2017). All efforts
948 were made to minimize animal suffering and the number of animals used.

949

950 **DATA AVAILABILITY**

951 All sequencing data that support the findings of this study have been deposited at
952 https://singlecell.broadinstitute.org/single_cell/reviewer_access/5a29ec20-d572-
953 4461-bfd3-cb8973c05f33 and are accessible through BioProject ID SCP1973.

954

## Acknowledgements

We thank Dr. Judith Konantz, M. Fischer, S. Kunadt and D. Mögel for excellent zebrafish care. We thank Katja Bernhardt for the excellent technical assistance in flow cytometry and cell sorting. We would like to thank also Susanne Reinhardt and Dr. Andreas Petzold from the DRESDEN-concept Genome Center for support with initial planning and bioinformatic processing of the scRNAseq experiment, respectively. We thank Prof. Marius Ader, Prof. Mike O. Karl, Dr. Volker Kroehne, Juliane Hammer and Elisa Nerli for critically reading the manuscript. In addition, we thank the members of the Brand laboratory for continued support and discussions as well as helpful comments on the manuscript. We thank also Dr. Christian Lange, Dr. Robert Münch and Dr. Steffen Rulands for excellent scientific discussion. This work was supported by grants to M.B. from the Deutsche Forschungsgemeinschaft (BR 1746/11-1), the European Union (European Research Council AdG Zf-BrainReg) and the German Excellence Initiative (Wissenschaftsrat and Deutsche Forschungsgemeinschaft) (EXC 168). Work was supported by the DRESDEN-concept Genome Center, the Light Microscopy Facility and Flow Cytometry Facility, core facilities of the CMCB at the Technische Universität Dresden. The funders had no role in study design, data collection and analysis, decision to publish, or preparation of the manuscript.

## Author contributions

Conceptualization: L.C, F.R., A.W., S.H., M.B.; Methodology: L.C., F.R., A.M., J.B., A.D.; Software: L.C., F.R., A.D., S.H., M.B.; Validation: L.C., F.R., A.M., J.B.; Formal analysis: L.C., F.R.; Investigation: L.C., F.R., A.M., J.B., A.D., S.H., and M.B; Resources: F.R., A.D., and M.B.; Data curation: L.C., F.R.; Writing - original draft

979 preparation: L.C., S.H., M.B.; Writing - review & editing: L.C., F.R., A.M., J.B., A.D.,
980 A.W., S.H., and M.B.; Project administration: M.B.; Funding acquisition: M.B.

981

982 **REFERENCES**


983 Agathocleous M, Harris WA. 2009. From progenitors to differentiated cells in the
984 vertebrate retina. *Annu Rev Cell Dev Biol* **25**:45–69.
985 doi:10.1146/annurev.cellbio.042308.113259

986 Aleström P, D'Angelo L, Midtlyng PJ, Schorderet DF, Schulte-Merker S, Sohm F,
987 Warner S. 2020. Zebrafish: Housing and husbandry recommendations. *Lab*
988 *Anim* **54**:213–224. doi:10.1177/0023677219869037

989 Alexiades MR, Cepko CL. 1997. Subsets of retinal progenitors display temporally
990 regulated and distinct biases in the fates of their progeny. *Development*
991 **124**:1119–1131. doi:10.1242/dev.124.6.1119

992 Amini R, Rocha-Martins M, Norden C. 2018. Neuronal Migration and Lamination in the
993 Vertebrate Retina. *Front Neurosci* **11**:742. doi:10.3389/fnins.2017.00742

994 Baraban M, Anselme I, Schneider-Maunoury S, Giudicelli F. 2013. Zebrafish
995 Embryonic Neurons Transport Messenger RNA to Axons and Growth Cones In
996 Vivo. *J Neurosci* **33**:15726–15734. doi:10.1523/JNEUROSCI.1510-13.2013

997 Bernardos RL, Barthel LK, Meyers JR, Raymond PA. 2007. Late-Stage Neuronal
998 Progenitors in the Retina Are Radial Muller Glia That Function as Retinal Stem
999 Cells. *Journal of Neuroscience* **27**:7028–7040. doi:10.1523/JNEUROSCI.1624-
1000 07.2007

1001 Bernardos RL, Raymond PA. 2006. GFAP transgenic zebrafish. *Gene Expr Patterns*
1002 **6**:1007–1013. doi:10.1016/j.modgep.2006.04.006

1003 Blackshaw S, Harpavat S, Trimarchi J, Cai L, Huang H, Kuo WP, Weber G, Lee K,
1004 Fraioli RE, Cho S-H, Yung R, Asch E, Ohno-Machado L, Wong WH, Cepko CL.

1005 2004. Genomic analysis of mouse retinal development. *PLoS Biol* **2**:E247.
1006 doi:10.1371/journal.pbio.0020247
1007 Brand, M., Granato, M. and Nüsslein-Volhard, C. (2002). Keeping and raising
1008 zebrafish. In Zebrafish: A Practical Approach, (ed. C. Nüsslein-Volhard and R.
1009 Dahm). Oxford: Oxford University Press.
1010 Buenaventura DF, Ghinia-Tegla MG, Emerson MM. 2018. Fate-restricted retinal
1011 progenitor cells adopt a molecular profile and spatial position distinct from
1012 multipotent progenitor cells. *Dev Biol* **443**:35–49.
1013 doi:10.1016/j.ydbio.2018.06.023
1014 Cameron DA, Gentile KL, Middleton FA, Yurco P. 2005. Gene expression profiles of
1015 intact and regenerating zebrafish retina. *Mol Vis* **11**:775–791.
1016 Campbell LJ, Levendusky JL, Steines SA, Hyde DR. 2022. Retinal regeneration
1017 requires dynamic Notch signaling. *Neural Regen Res* **17**:1199–1209.
1018 doi:10.4103/1673-5374.327326
1019 Cepko C. 2014. Intrinsically different retinal progenitor cells produce specific types of
1020 progeny. *Nat Rev Neurosci* **15**:615–627. doi:10.1038/nrn3767
1021 Cepko CL, Austin CP, Yang X, Alexiades M, Ezzeddine D. 1996. Cell fate
1022 determination in the vertebrate retina. *PNAS* **93**:589–595.
1023 doi:10.1073/pnas.93.2.589
1024 Corso-Díaz X, Simpson EM. 2015. Nr2e1 regulates retinal lamination and the
1025 development of Müller glia, S-cones, and glycineric amacrine cells during
1026 retinogenesis. *Molecular Brain* **8**:37. doi:10.1186/s13041-015-0126-x
1027 Craig SEL, Calinescu A-A, Hitchcock PF. 2008. Identification of the molecular
1028 signatures integral to regenerating photoreceptors in the retina of the zebra fish.
1029 *j ocul biol dis inform* **1**:73–84. doi:10.1007/s12177-008-9011-5

1030 D'Aniello E, Ravisankar P, Waxman JS. 2015. Rdh10a Provides a Conserved Critical
1031 Step in the Synthesis of Retinoic Acid during Zebrafish Embryogenesis. *PLOS*
1032 *ONE* **10**:e0138588. doi:10.1371/journal.pone.0138588
1033 Dowling JE. 1987. The Retina: An Approachable Part of the Brain. Harvard University
1034 Press.
1035 Emerson MM, Surzenko N, Goetz JJ, Trimarchi J, Cepko CL. 2013. Otx2 and Onecut1
1036 promote the fates of cone photoreceptors and horizontal cells and repress rod
1037 photoreceptors. *Dev Cell* **26**:59–72. doi:10.1016/j.devcel.2013.06.005
1038 Fausett BV, Goldman D. 2006. A Role for 1 Tubulin-Expressing Muller Glia in
1039 Regeneration of the Injured Zebrafish Retina. *Journal of Neuroscience*
1040 **26**:6303–6313. doi:10.1523/JNEUROSCI.0332-06.2006
1041 Fausett BV, Gumerson JD, Goldman D. 2008. The Proneural Basic Helix-Loop-Helix
1042 Gene Ascl1a Is Required for Retina Regeneration. *Journal of Neuroscience*
1043 **28**:1109–1117. doi:10.1523/JNEUROSCI.4853-07.2008
1044 Feng L, Hernandez RE, Waxman JS, Yelon D, Moens CB. 2010. Dhrs3a regulates
1045 retinoic acid biosynthesis through a feedback inhibition mechanism.
1046 *Developmental Biology* **338**:1–14. doi:10.1016/j.ydbio.2009.10.029
1047 Fimbel SM, Montgomery JE, Burket CT, Hyde DR. 2007. Regeneration of Inner Retinal
1048 Neurons after Intravitreal Injection of Ouabain in Zebrafish. *Journal of*
1049 *Neuroscience* **27**:1712–1724. doi:10.1523/JNEUROSCI.5317-06.2007
1050 Fleisch VC, Fraser B, Allison WT. 2011. Investigating regeneration and functional
1051 integration of CNS neurons: Lessons from zebrafish genetics and other fish
1052 species. *Biochimica et Biophysica Acta (BBA) - Molecular Basis of Disease*
1053 **1812**:364–380. doi:10.1016/j.bbadis.2010.10.012
1054 Godinho L, Williams PR, Claassen Y, Provost E, Leach SD, Kamermans M, Wong
1055 ROL. 2007. Nonapical Symmetric Divisions Underlie Horizontal Cell Layer

1056 Formation in the Developing Retina In Vivo. *Neuron* **56**:597–603.
1057 doi:10.1016/j.neuron.2007.09.036
1058 Gorsuch RA, Hyde DR. 2014. Regulation of Müller glial dependent neuronal
1059 regeneration in the damaged adult zebrafish retina. *Experimental Eye Research*
1060 **123**:131–140. doi:10.1016/j.exer.2013.07.012
1061 Gorsuch RA, Lahne M, Yarka CE, Petravick ME, Li J, Hyde DR. 2017. Sox2 regulates
1062 Müller glia reprogramming and proliferation in the regenerating zebrafish retina
1063 via Lin28 and Ascl1a. *Exp Eye Res* **161**:174–192.
1064 doi:10.1016/j.exer.2017.05.012
1065 Grandel H, Kaslin J, Ganz J, Wenzel I, Brand M. 2006. Neural stem cells and
1066 neurogenesis in the adult zebrafish brain: Origin, proliferation dynamics,
1067 migration and cell fate. *Developmental Biology* **295**:263–277.
1068 doi:10.1016/j.ydbio.2006.03.040
1069 Hoang T, Wang J, Boyd P, Wang F, Santiago C, Jiang L, Yoo S, Lahne M, Todd LJ,
1070 Jia M, Saez C, Keuthan C, Palazzo I, Squires N, Campbell WA, Rajaii F, Parayil
1071 T, Trinh V, Kim DW, Wang G, Campbell LJ, Ash J, Fischer AJ, Hyde DR, Qian
1072 J, Blackshaw S. 2020. Gene regulatory networks controlling vertebrate retinal
1073 regeneration. *Science* **370**:eabb8598. doi:10.1126/science.abb8598
1074 Holmes RS, Hempel J. 2011. Comparative studies of vertebrate aldehyde
1075 dehydrogenase 3: Sequences, structures, phylogeny and evolution. Evidence
1076 for a mammalian origin for the ALDH3A1 gene. *Chemico-Biological Interactions*,
1077 Enzymology and Molecular Biology of Carbonyl Metabolism **191**:113–121.
1078 doi:10.1016/j.cbi.2011.01.014
1079 Hoon M, Okawa H, Santina LD, Wong ROL. 2014. Functional Architecture of the
1080 Retina: Development and Disease. *Prog Retin Eye Res* **42**:44–84.
1081 doi:10.1016/j.preteyeres.2014.06.003

1082 Javed A, Cayouette M. 2017. Temporal Progression of Retinal Progenitor Cell Identity:
1083 Implications in Cell Replacement Therapies. *Frontiers in Neural Circuits* **11**.
1084 Jusuf PR, Almeida AD, Randlett O, Joubin K, Poggi L, Harris WA. 2011. Origin and
1085 Determination of Inhibitory Cell Lineages in the Vertebrate Retina. *J Neurosci*
1086 **31**:2549–2562. doi:10.1523/JNEUROSCI.4713-10.2011
1087 Jusuf PR, Harris WA. 2009. Ptf1a is expressed transiently in all types of amacrine cells
1088 in the embryonic zebrafish retina. *Neural Dev* **4**:34. doi:10.1186/1749-8104-4-
1089 34
1090 Kassen SC, Ramanan V, Montgomery JE, T. Burket C, Liu C-G, Vihtelic TS, Hyde DR.
1091 2007. Time course analysis of gene expression during light-induced
1092 photoreceptor cell death and regeneration in *albino* zebrafish. *Devel Neurobio*
1093 **67**:1009–1031. doi:10.1002/dneu.20362
1094 Kitambi SS, Hauptmann G. 2007. The zebrafish orphan nuclear receptor genes nr2e1
1095 and nr2e3 are expressed in developing eye and forebrain. *Gene Expression*
1096 *Patterns* **7**:521–528. doi:10.1016/j.modgep.2006.10.006
1097 Klimova L, Antosova B, Kuzelova A, Strnad H, Kozmik Z. 2015. Onecut1 and Onecut2
1098 transcription factors operate downstream of Pax6 to regulate horizontal cell
1099 development. *Developmental Biology* **402**:48–60.
1100 doi:10.1016/j.ydbio.2015.02.023
1101 Kramer AC, Gurdziel K, Thummel R. 2021. A Comparative Analysis of Gene and
1102 Protein Expression Throughout a Full 28-Day Retinal Regeneration Time-
1103 Course in Adult Zebrafish. *Front Cell Dev Biol* **9**:741514.
1104 doi:10.3389/fcell.2021.741514
1105 Kroehne V, Freudenreich D, Hans S, Kaslin J, Brand M. 2011. Regeneration of the
1106 adult zebrafish brain from neurogenic radial glia-type progenitors. *Development*
1107 **138**:4831–4841. doi:10.1242/dev.072587

1108 Lahne M, Brecker M, Jones SE, Hyde DR. 2020a. The Regenerating Adult Zebrafish
1109 Retina Recapitulates Developmental Fate Specification Programs. *Front Cell*
1110 *Dev Biol* **8**:617923. doi:10.3389/fcell.2020.617923
1111 Lahne M, Li J, Marton RM, Hyde DR. 2015. Actin-Cytoskeleton- and Rock-Mediated
1112 INM Are Required for Photoreceptor Regeneration in the Adult Zebrafish Retina.
1113 *J Neurosci* **35**:15612–15634. doi:10.1523/JNEUROSCI.5005-14.2015
1114 Lahne M, Nagashima M, Hyde DR, Hitchcock PF. 2020b. Reprogramming Müller Glia
1115 to Regenerate Retinal Neurons. *Annu Rev Vis Sci* **6**:171–193.
1116 doi:10.1146/annurev-vision-121219-081808
1117 Lange C, Rost F, Machate A, Reinhardt S, Lesche M, Weber A, Kuscha V, Dahl A,
1118 Rulands S, Brand M. 2020. Single cell sequencing of radial glia progeny reveals
1119 diversity of newborn neurons in the adult zebrafish brain. *Development*
1120 1855951. doi:10.1242/dev.185595
1121 Lenkowski JR, Raymond PA. 2014. Müller glia: Stem cells for generation and
1122 regeneration of retinal neurons in teleost fish. *Progress in Retinal and Eye*
1123 *Research* **40**:94–123. doi:10.1016/j.preteyeres.2013.12.007
1124 Livesey FJ, Cepko CL. 2001. Vertebrate neural cell-fate determination: lessons from
1125 the retina. *Nat Rev Neurosci* **2**:109–118. doi:10.1038/35053522
1126 Lun ATL, McCarthy DJ, Marioni JC. 2016. A step-by-step workflow for low-level
1127 analysis of single-cell RNA-seq data with Bioconductor.
1128 doi:10.12688/f1000research.9501.2
1129 Macosko EZ, Basu A, Satija R, Nemesh J, Shekhar K, Goldman M, Tirosh I, Bialas
1130 AR, Kamitaki N, Martersteck EM, Trombetta JJ, Weitz DA, Sanes JR, Shalek
1131 AK, Regev A, McCarroll SA. 2015. Highly Parallel Genome-wide Expression
1132 Profiling of Individual Cells Using Nanoliter Droplets. *Cell* **161**:1202–1214.
1133 doi:10.1016/j.cell.2015.05.002

1134 Morris AC, Forbes-Osborne MA, Pillai LS, Fadool JM. 2011. Microarray Analysis of
1135 XOPS-mCFP Zebrafish Retina Identifies Genes Associated with Rod
1136 Photoreceptor Degeneration and Regeneration. *Investigative Ophthalmology &*
1137 *Visual Science* **52**:2255–2266. doi:10.1167/iovs.10-6022
1138 Morris AC, Schroeter EH, Bilotta J, Wong ROL, Fadool JM. 2005. Cone survival
1139 despite rod degeneration in XOPS-mCFP transgenic zebrafish. *Invest*
1140 *Ophthalmol Vis Sci* **46**:4762–4771. doi:10.1167/iovs.05-0797
1141 Mu Z, Zhang S, He C, Hou H, Liu D, Hu N, Xu H. 2016. Expression of SoxC
1142 Transcription Factors during Zebrafish Retinal and Optic Nerve Regeneration.
1143 *Neurosci Bull* **33**:53–61. doi:10.1007/s12264-016-0073-2
1144 Muto A, Iida A, Satoh S, Watanabe S. 2009. The group E Sox genes Sox8 and Sox9
1145 are regulated by Notch signaling and are required for Müller glial cell
1146 development in mouse retina. *Exp Eye Res* **89**:549–558.
1147 doi:10.1016/j.exer.2009.05.006
1148 Nagashima M, Barthel LK, Raymond PA. 2013. A self-renewing division of zebrafish
1149 Müller glial cells generates neuronal progenitors that require N-cadherin to
1150 regenerate retinal neurons. *Development* **140**:4510–4521.
1151 doi:10.1242/dev.090738
1152 Nelson CM, Ackerman KM, O'Hayer P, Bailey TJ, Gorsuch RA, Hyde DR. 2013. Tumor
1153 Necrosis Factor-Alpha Is Produced by Dying Retinal Neurons and Is Required
1154 for Muller Glia Proliferation during Zebrafish Retinal Regeneration. *Journal of*
1155 *Neuroscience* **33**:6524–6539. doi:10.1523/JNEUROSCI.3838-12.2013
1156 Nerli E, Kretzschmar J, Bianucci T, Rocha-Martins M, Zechner C, Norden C. 2022.
1157 Deterministic and probabilistic fate decisions co-exist in a single retinal lineage.
1158 doi:10.1101/2022.08.11.503564

1159 Ng Chi Kei J, Currie PD, Jusuf PR. 2017. Fate bias during neural regeneration adjusts
1160 dynamically without recapitulating developmental fate progression. *Neural Dev*
1161 **12**:12. doi:10.1186/s13064-017-0089-y
1162 Peterson RE, Fadool JM, Mcclintock J, Linser PJ. 2001. Müller cell differentiation in
1163 the zebrafish neural retina: Evidence of distinct early and late stages in cell
1164 maturation. *Journal of Comparative Neurology* **429**:530–540. doi:10.1002/1096-
1165 9861(20010122)429:4<530::AID-CNE2>3.0.CO;2-C
1166 Poché RA, Furuta Y, Chaboissier M-C, Schedl A, Behringer RR. 2008. Sox9 is
1167 expressed in mouse multipotent retinal progenitor cells and functions in Müller
1168 Glial cell development. *Journal of Comparative Neurology* **510**:237–250.
1169 doi:10.1002/cne.21746
1170 Poggi L, Vitorino M, Masai I, Harris WA. 2005. Influences on neural lineage and mode
1171 of division in the zebrafish retina in vivo. *J Cell Biol* **171**:991–999.
1172 doi:10.1083/jcb.200509098
1173 Powell C, Cornblath E, Elsaeidi F, Wan J, Goldman D. 2016. Zebrafish Müller glia-
1174 derived progenitors are multipotent, exhibit proliferative biases and regenerate
1175 excess neurons. *Sci Rep* **6**:24851. doi:10.1038/srep24851
1176 Qin Z, Barthel LK, Raymond PA. 2009. Genetic evidence for shared mechanisms of
1177 epimorphic regeneration in zebrafish. *Proc Natl Acad Sci U S A* **106**:9310–9315.
1178 doi:10.1073/pnas.0811186106
1179 Ramachandran R, Reifler A, Parent JM, Goldman D. 2010. Conditional gene
1180 expression and lineage tracing of tuba1a expressing cells during zebrafish
1181 development and retina regeneration. *J Comp Neurol* **518**:4196–4212.
1182 doi:10.1002/cne.22448

1183 Ramachandran R, Zhao X-F, Goldman D. 2012. Insm1a-mediated gene repression is
1184 essential for the formation and differentiation of Müller glia-derived progenitors
1185 in the injured retina. *Nat Cell Biol* **14**:1013–1023. doi:10.1038/ncb2586
1186 Ramachandran R, Zhao X-F, Goldman D. 2011. Ascl1a/Dkk/ -catenin signaling
1187 pathway is necessary and glycogen synthase kinase-3 inhibition is sufficient for
1188 zebrafish retina regeneration. *Proceedings of the National Academy of*
1189 *Sciences* **108**:15858–15863. doi:10.1073/pnas.1107220108
1190 Raymond PA, Barthel LK, Bernardos RL, Perkowski JJ. 2006. Molecular
1191 characterization of retinal stem cells and their niches in adult zebrafish. *BMC*
1192 *Dev Biol* **6**:36. doi:10.1186/1471-213X-6-36
1193 Saade CJ, Alvarez-Delfin K, Fadool JM. 2013. Rod photoreceptors protect from cone
1194 degeneration-induced retinal remodeling and restore visual responses in
1195 zebrafish. *J Neurosci* **33**:1804–1814. doi:10.1523/JNEUROSCI.2910-12.2013
1196 Sapkota D, Chintala H, Wu F, Fliesler SJ, Hu Z, Mu X. 2014. Onecut1 and Onecut2
1197 redundantly regulate early retinal cell fates during development. *PNAS*
1198 **111**:E4086–E4095. doi:10.1073/pnas.1405354111
1199 Schindelin J, Arganda-Carreras I, Frise E, Kaynig V, Longair M, Pietzsch T, Preibisch
1200 S, Rueden C, Saalfeld S, Schmid B, Tinevez J-Y, White DJ, Hartenstein V,
1201 Eliceiri K, Tomancak P, Cardona A. 2012. Fiji: an open-source platform for
1202 biological-image analysis. *Nat Methods* **9**:676–682. doi:10.1038/nmeth.2019
1203 Sherpa T, Fimbel SM, Mallory DE, Maaswinkel H, Spritzer SD, Sand JA, Li L, Hyde
1204 DR, Stenkamp DL. 2008. Ganglion cell regeneration following whole-retina
1205 destruction in zebrafish. *Devel Neurobio* **68**:166–181. doi:10.1002/dneu.20568
1206 Silva NJ, Nagashima M, Li J, Kakuk-Atkins L, Ashrafzadeh M, Hyde DR, Hitchcock PF.
1207 2020. Inflammation and matrix metalloproteinase 9 (Mmp-9) regulate

1208 photoreceptor regeneration in adult zebrafish. *Glia* **68**:1445–1465.
1209 doi:10.1002/glia.23792
1210 Stenkamp DL. 2015. Development of the Vertebrate Eye and Retina. *Prog Mol Biol*
1211 *Transl Sci* **134**:397–414. doi:10.1016/bs.pmbts.2015.06.006
1212 Stenkamp DL. 2011. The rod photoreceptor lineage of teleost fish. *Progress in Retinal*
1213 *and Eye Research* **30**:395–404. doi:10.1016/j.preteyeres.2011.06.004
1214 Stenkamp DL. 2007. Neurogenesis in the fish retina. *Int Rev Cytol* **259**:173–224.
1215 doi:10.1016/S0074-7696(06)59005-9
1216 Suzuki SC, Bleckert A, Williams PR, Takechi M, Kawamura S, Wong ROL. 2013. Cone
1217 photoreceptor types in zebrafish are generated by symmetric terminal divisions
1218 of dedicated precursors. *PNAS* **110**:15109–15114.
1219 doi:10.1073/pnas.1303551110
1220 Thummel R, Enright JM, Kassen SC, Montgomery JE, Bailey TJ, Hyde DR. 2010.
1221 Pax6a and Pax6b are required at different points in neuronal progenitor cell
1222 proliferation during zebrafish photoreceptor regeneration. *Experimental Eye*
1223 *Research* **90**:572–582. doi:10.1016/j.exer.2010.02.001
1224 Thummel R, Kassen SC, Enright JM, Nelson CM, Montgomery JE, Hyde DR. 2008.
1225 Characterization of Müller glia and neuronal progenitors during adult zebrafish
1226 retinal regeneration. *Experimental Eye Research* **87**:433–444.
1227 doi:10.1016/j.exer.2008.07.009
1228 Tirosh I, Izar B, Prakadan SM, Wadsworth MH, Treacy D, Trombetta JJ, Rotem A,
1229 Rodman C, Lian C, Murphy G, Fallahi-Sichani M, Dutton-Regester K, Lin J-R,
1230 Cohen O, Shah P, Lu D, Genshaft AS, Hughes TK, Ziegler CGK, Kazer SW,
1231 Gaillard A, Kolb KE, Villani A-C, Johannessen CM, Andreev AY, Van Allen EM,
1232 Bertagnolli M, Sorger PK, Sullivan RJ, Flaherty KT, Frederick DT, Jané-
1233 Valbuena J, Yoon CH, Rozenblatt-Rosen O, Shalek AK, Regev A, Garraway

1234 LA. 2016. Dissecting the multicellular ecosystem of metastatic melanoma by
1235 single-cell RNA-seq. *Science* **352**:189–196. doi:10.1126/science.aad0501
1236 Turner DL, Cepko CL. 1987. A common progenitor for neurons and glia persists in rat
1237 retina late in development. *Nature* **328**:131–136. doi:10.1038/328131a0
1238 Vihtelic TS, Hyde DR. 2000. Light-induced rod and cone cell death and regeneration
1239 in the adult albino zebrafish (Danio rerio) retina. *J Neurobiol* **44**:289–307.
1240 doi:10.1002/1097-4695(20000905)44:3<289::aid-neu1>3.0.co;2-h
1241 Vihtelic TS, Soverly JE, Kassen SC, Hyde DR. 2006. Retinal regional differences in
1242 photoreceptor cell death and regeneration in light-lesioned albino zebrafish.
1243 *Experimental Eye Research* **82**:558–575. doi:10.1016/j.exer.2005.08.015
1244 Wan J, Goldman D. 2016. Retina regeneration in zebrafish. *Curr Opin Genet Dev*
1245 **40**:41–47. doi:10.1016/j.gde.2016.05.009
1246 Wan J, Ramachandran R, Goldman D. 2012. HB-EGF Is Necessary and Sufficient for
1247 Müller Glia Dedifferentiation and Retina Regeneration. *Developmental Cell*
1248 **22**:334–347. doi:10.1016/j.devcel.2011.11.020
1249 Weber A, Hochmann S, Cimalla P, Gärtner M, Kuscha V, Hans S, Geffarth M, Kaslin
1250 J, Koch E, Brand M. 2013. Characterization of light lesion paradigms and optical
1251 coherence tomography as tools to study adult retina regeneration in zebrafish.
1252 *PLoS One* **8**:e80483. doi:10.1371/journal.pone.0080483
1253 Weber IP, Ramos AP, Strzyz PJ, Leung LC, Young S, Norden C. 2014. Mitotic Position
1254 and Morphology of Committed Precursor Cells in the Zebrafish Retina Adapt to
1255 Architectural Changes upon Tissue Maturation. *Cell Reports* **7**:386–397.
1256 doi:10.1016/j.celrep.2014.03.014
1257 Whitfield ML, Sherlock G, Saldanha AJ, Murray JI, Ball CA, Alexander KE, Matese JC,
1258 Perou CM, Hurt MM, Brown PO, Botstein D. 2002. Identification of genes

1259 periodically expressed in the human cell cycle and their expression in tumors.
1260 *Mol Biol Cell* **13**:1977–2000. doi:10.1091/mbc.02-02-0030
1261 Wilson SG, Wen W, Pillai-Kastoori L, Morris AC. 2016. Tracking the fate of her4
1262 expressing cells in the regenerating retina using her4:Kaede zebrafish. *Exp Eye*
1263 *Res* **145**:75–87. doi:10.1016/j.exer.2015.11.002
1264 Wu F, Bard JE, Kann J, Yergeau D, Sapkota D, Ge Y, Hu Z, Wang J, Liu T, Mu X.
1265 2021. Single cell transcriptomics reveals lineage trajectory of retinal ganglion
1266 cells in wild-type and Atoh7-null retinas. *Nat Commun* **12**:1465.
1267 doi:10.1038/s41467-021-21704-4
1268 Xu B, Tang X, Jin M, Zhang H, Du L, Yu S, He J. 2020. Unifying developmental
1269 programs for embryonic and postembryonic neurogenesis in the zebrafish
1270 retina. *Development* **147**:dev185660. doi:10.1242/dev.185660
1271 Young RW. 1985. Cell differentiation in the retina of the mouse. *Anat Rec* **212**:199–
1272 205. doi:10.1002/ar.1092120215
1273 Yurco P, Cameron DA. 2005. Responses of Müller glia to retinal injury in adult
1274 zebrafish. *Vision Research* **45**:991–1002. doi:10.1016/j.visres.2004.10.022
1275 Zhang Y, Buchholz F, Muyrers JPP, Stewart AF. 1998. A new logic for DNA
1276 engineering using recombination in Escherichia coli. *Nat Genet* **20**:123–128.
1277 doi:10.1038/2417
1278 Zhao X-F, Wan J, Powell C, Ramachandran R, Myers MG, Goldman D. 2014. Leptin
1279 and IL-6 family cytokines synergize to stimulate Müller glia reprogramming and
1280 retina regeneration. *Cell Rep* **9**:272–284. doi:10.1016/j.celrep.2014.08.047
1281 Zheng GXY, Terry JM, Belgrader P, Ryvkin P, Bent ZW, Wilson R, Ziraldo SB, Wheeler
1282 TD, McDermott GP, Zhu J, Gregory MT, Shuga J, Montesclaros L, Underwood
1283 JG, Masquelier DA, Nishimura SY, Schnall-Levin M, Wyatt PW, Hindson CM,
1284 Bharadwaj R, Wong A, Ness KD, Beppu LW, Deeg HJ, McFarland C, Loeb KR,

1285 Valente WJ, Ericson NG, Stevens EA, Radich JP, Mikkelsen TS, Hindson BJ,
1286 Bielas JH. 2017. Massively parallel digital transcriptional profiling of single cells.
1287 *Nat Commun* **8**:14049. doi:10.1038/ncomms14049

1288

1289

1290 **SUPPLEMENTAL FIGURES**

1291 **Figure 1-figure supplement 1:** characterization of the fluorescent reporter lines
1292 *Tg(pcna:EGFP)* and *Tg(gfap:mCherry)* in double transgenic animals.

1293 **Figure 1-figure supplement 2:** expression profile of
1294 *Tg(pcna:EGFP);Tg(gfap:mCherry)* during retina regeneration.

1295 **Figure 1-figure supplement 3:** fluorescence activated cell sorting (FACS) and gating
1296 strategies.

1297 **Figure 2-figure supplement 1:** original scRNAseq dataset

1298 **Figure 2-figure supplement 2:** dot plot of top 5 marker genes per cluster.

1299 **Figure 3-figure supplement 1:** expression of selected genes per cluster.

1300 **Figure 8-figure supplement 1:** birthdate order of regenerated progeny.

1301 **Figure 8-figure supplement 2:** expression of mature markers.

1302

1303 **SUPPLEMENTARY FILES**

1304 **Key_resource_table:** materials, antibodies and reagents

1305 **Supplementary file 1:** Top 100 marker genes per cluster

1306 **Supplementary file 2:** Top 100 differentially expressed genes between Non-reactive
1307 Müller glia (1) and Non-reactive Müller glia (2)

1308 **Supplementary file 3:** Top 100 differentially expressed genes between Reactive
1309 Müller glia (1) and Reactive Müller glia (2)

1310 **Supplementary file 4:** Top 100 differentially expressed genes between Reactive
1311 Müller glia (1) and Müller glia/Progenitors 1

1312 **Supplementary file 5:** Top 100 differentially expressed genes between Reactive
1313 Müller glia (2) and Müller glia/Progenitors 1

1314 **Supplementary file 6:** Top 100 differentially expressed genes between Müller
1315 glia/Progenitors 1 and Progenitors 2

Figure 1

A

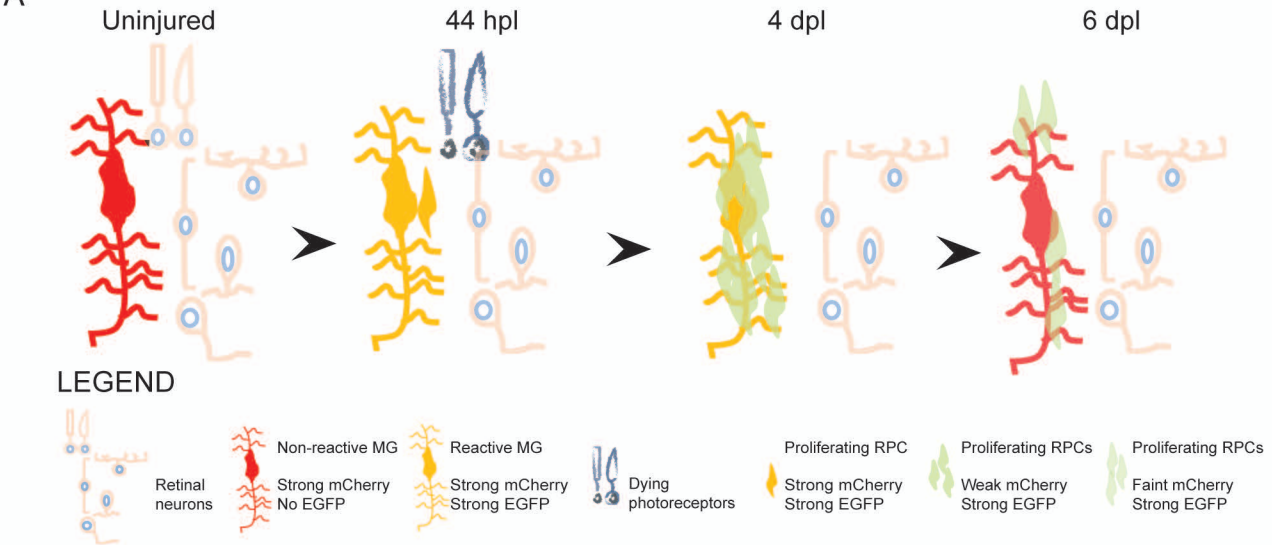
Uninjured
44 hpl
4 dpl
6 dpl
LEGEND
Retinal neurons
Non-reactive MG
Strong mCherry
No EGFP
Reactive MG
Strong mCherry
Strong EGFP
Dying photoreceptors
Proliferating RPC
Strong mCherry
Strong EGFP
Proliferating RPCs
Weak mCherry
Strong EGFP
Proliferating RPCs
Faint mCherry
Strong EGFP

B

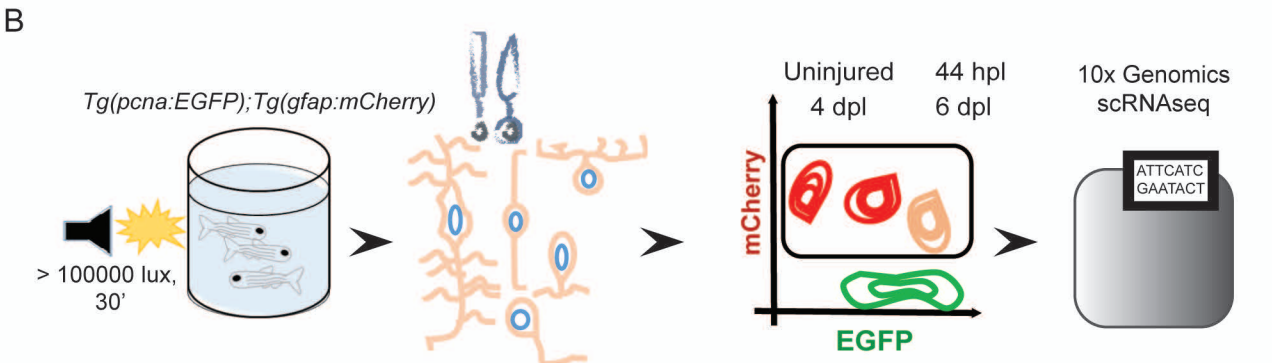
Tg(pcna:EGFP);Tg(gfap:mCherry)
> 100000 lux,
30'
Uninjured
4 dpl
44 hpl
6 dpl
mCherry
EGFP
10x Genomics
scRNAseq
ATTCATC
GAATACT

C

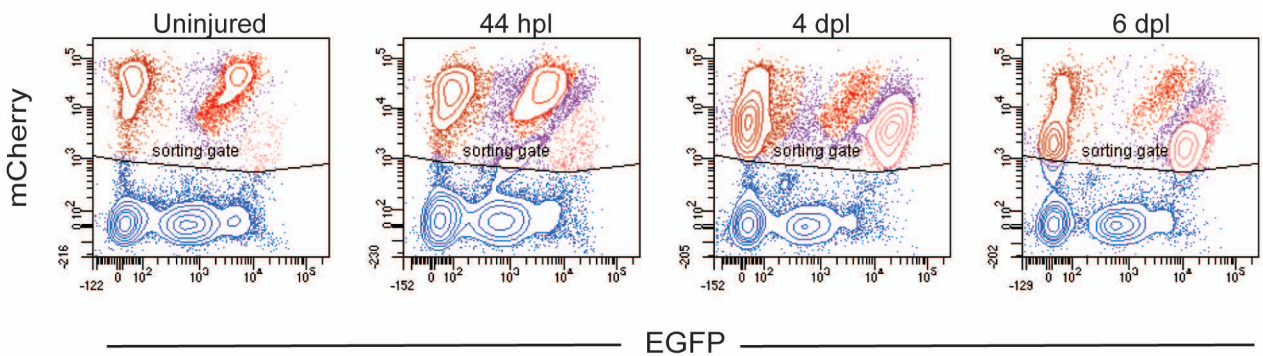
Uninjured
44 hpl
4 dpl
6 dpl
mCherry
sorting gate
EGFP

**Figure 1: Isolation of individual MG, RPCs and regenerated progeny using fluorescent reporters. (A)** Schematic illustration of the rationale to isolate individual cells from regenerating retinae of double transgenic *Tg(pcna:EGFP);Tg(gfap:mCherry)* animals. In the uninjured retina, MG express strong levels of mCherry but no EGFP. Upon light lesion, which results in dying photoreceptors, MG turn on EGFP resulting in the presence of both fluorophores at 44 hours post lesion (hpl). At 4 days post lesion (dpl), MG remain to contain strong mCherry and EGFP levels. In contrast, further proliferating RPCs display weak mCherry but strong EGFP fluorescence. Finally, MG have lost the EGFP signal at 6 dpl, expressing mCherry only. RPCs, which start to migrate and differentiate, are still detectable but show diluted levels of mCherry and EGFP. **(B)** Schematic illustration of the workflow for the scRNAseq experiment. Uninjured control and light lesioned retinae (44 hpl, 4 dpl, 6 dpl) of double transgenic *Tg(pcna:EGFP);Tg(gfap:mCherry)* animals were dissociated to obtain a single cell suspension. Following fluorescent activated cell sorting of mCherry-positive only and EGFP/mCherry-double positive cells, individual cells were eventually subjected to droplet-based, 10x Genomics scRNAseq. **(C)** Flow cytometry plots depicting EGFP and mCherry fluorescence of dissociated retinal cells at the indicated time points. Cells in the sorting gate include mCherry-positive only as well as mCherry/EGFP-double positive cells. Number of cells sorted from the sorting gate per time point: 15.000. **Associated: supplemental figures 1, 2 and 3.**

Figure 2

A

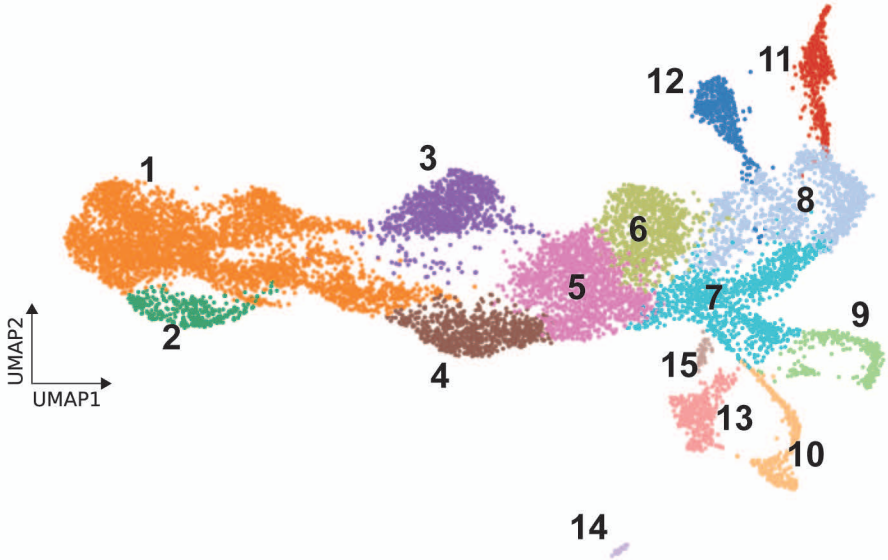


1. Non-reactive Müller glia 1
2. Non-reactive Müller glia 2
3. Reactive Müller glia 1
4. Reactive Müller glia 2
5. Müller glia/Progenitors 1
6. Progenitors 2
7. Progenitors 3
8. Photoreceptor precursors
9. Horizontal cell precursors
10. Retinal ganglion cells
11. Red cones
12. Blue cones
13. Amacrine cells 1
14. Amacrine cells 2
15. Bipolar cells

B

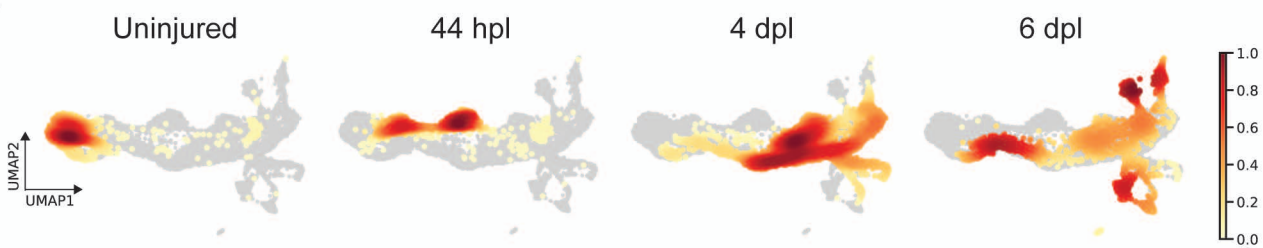


C

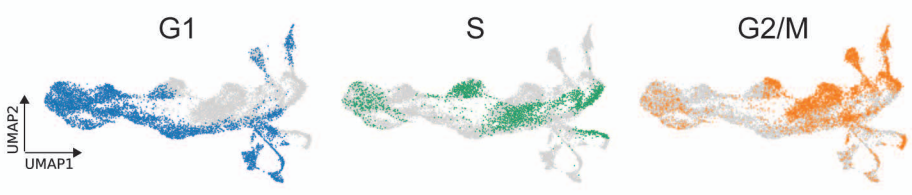


D

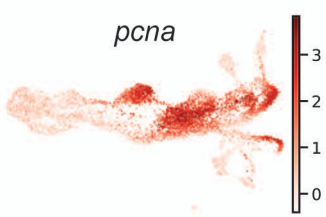

**Figure 2: scRNAseq identifies 15 different cell populations in the light-lesioned retina. (A)** 11.690 cells depicted on the uniform manifold approximation and projection (UMAP) map. From left to right, the map shows a progressive emergence of MG, RPCs and progeny clusters. See figure legend for the detailed information about cluster identity. **(B)** Normalized cell density on the UMAP for the 4 different samples (uninjured, 44 hpl, 4 and 6 dpl). Dark red shows strong cell enrichment and no color absence of cells. **(C)** Cells colored by cell cycle phases (G1, S, and G2/M phase in blue, green and orange, respectively). **(D)** Expression of *pcna*. Legend: logarithm of normalized counts per million. **Associated: supplemental figures 1 and 2.**

Figure 3

A

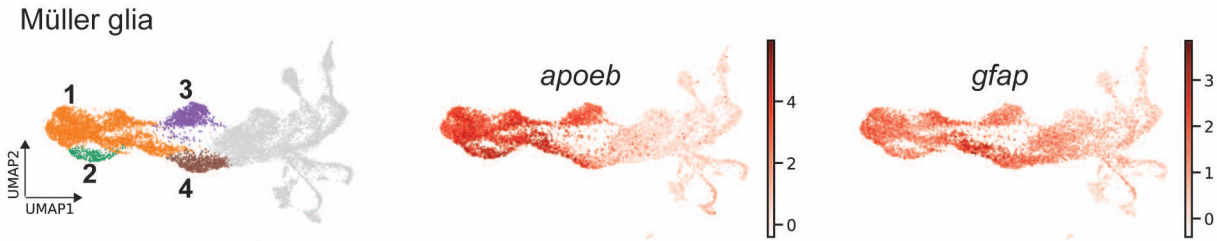


B

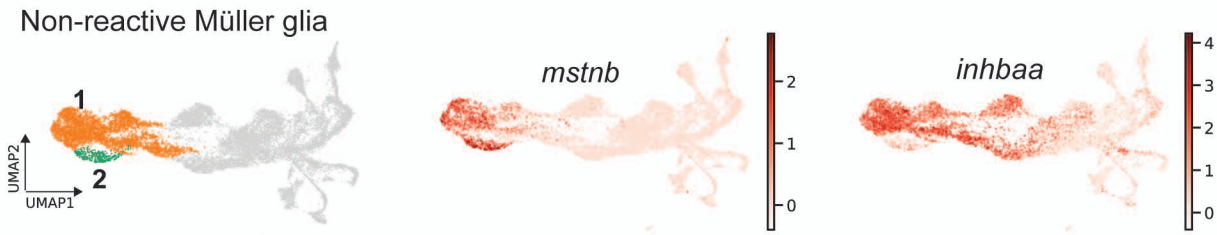


C

D

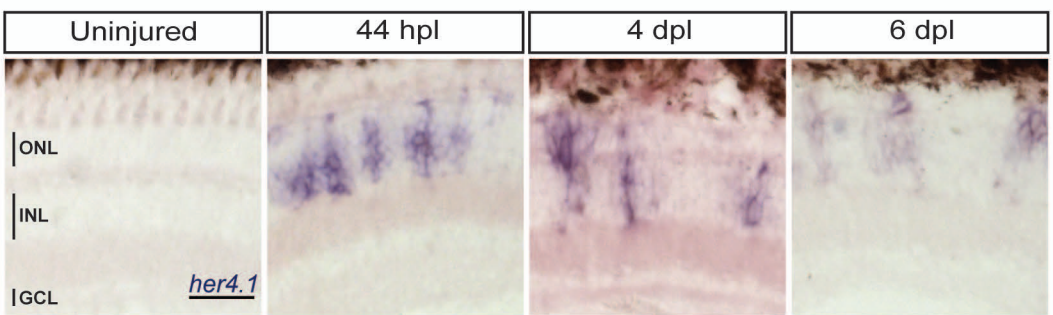

**Figure 3: scRNAseq reveals heterogeneity in Müller glia and identifies two populations of non-reactive and two of reactive Müller glia in the light-lesioned retina. (A)** Four Müller glia clusters (cluster 1-4) and the expression levels of *apoeb* and *gfap*. **(B)** The two non-reactive Müller glia clusters (cluster 1 and 2) and the expression levels of *mstnb* and *inhbaa*. Cells of both clusters express *mstnb*, but only cells in cluster 1 expresses *inhbaa*. **(C)** Visualization of the two reactive Müller glia clusters (cluster 3 and 4) and the relative expression levels of *crlf1a* and *her4.1* projected onto the main transcriptional UMAP. Cells of both clusters express *crlf1a*, but only cells in cluster 3 expresses *her4.1*. **(D)** Bright field microscopy images of chromogenic *in situ* hybridization detecting *her4.1* on retinal sections of uninjured control animals and at 44 hours post lesion (hpl), 4 days post lesion (dpl) and 6 dpl. N= 3 fish per time point and uninjured controls. The position of the outer nuclear layer (ONL), inner nuclear layer (INL) and ganglion cell layer (GCL) is indicated in the uninjured sample. Scale bar: 30 µm. **Associated: supplemental figure 1.**

Figure 4

A

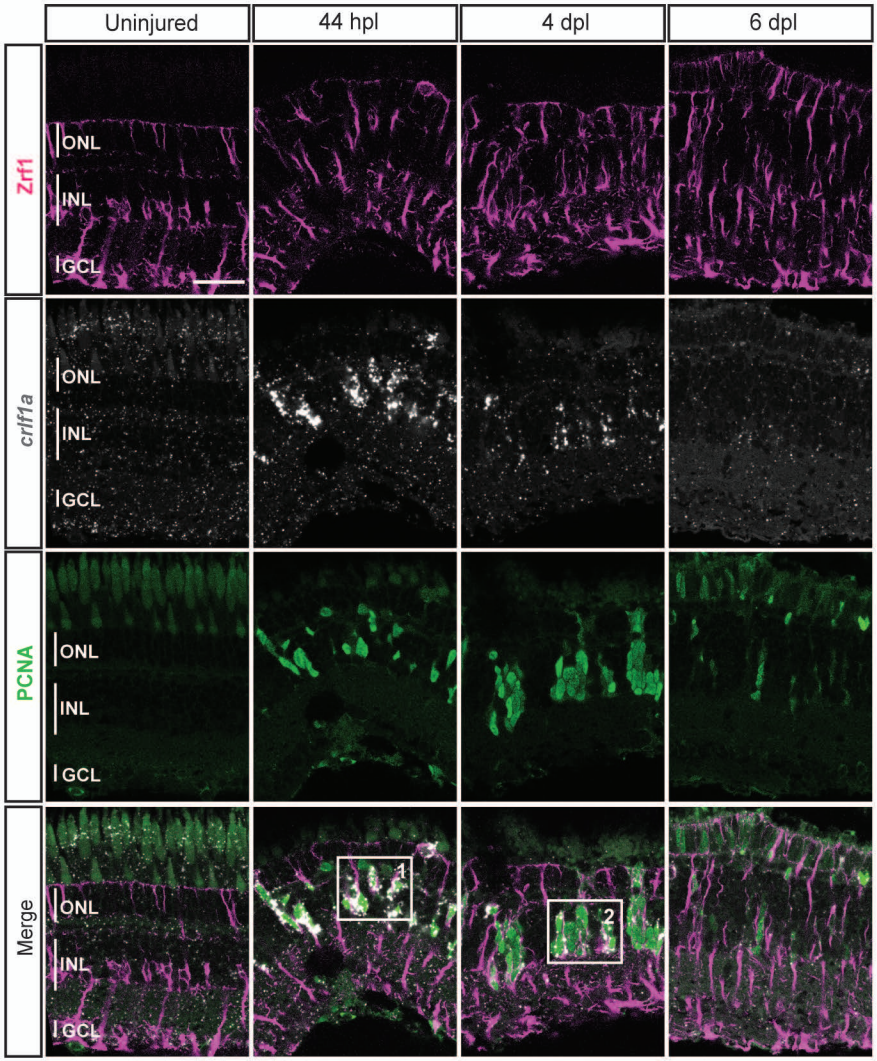
Uninjured
44 hpl
4 dpl
6 dpl
Zrf1
crlf1a
PCNA
Merge
ONL
INL
GCL
1
2

B

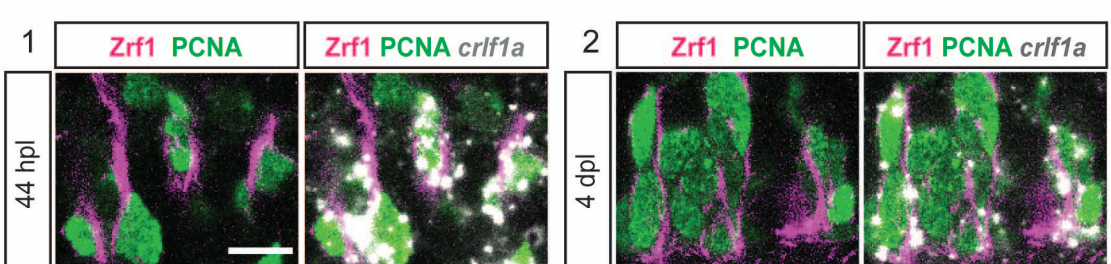
1
Zrf1 PCNA
Zrf1 PCNA crlf1a
44 hpl
2
Zrf1 PCNA
Zrf1 PCNA crlf1a
4 dpl

**Figure 4: expression profile of *crlf1a* during retina regeneration. (A)** Confocal images of fluorescent *in situ* hybridization for *crlf1a* (grey) and immunohistochemistry detecting Zrf1-positive MG fibers (magenta) and the proliferation marker PCNA (green) on retinal sections of uninjured control animals and at 44 hours post lesion (hpl), 4 days post lesion (dpl) and 6 dpl. The position of the outer nuclear layer (ONL), inner nuclear laser (INL) and ganglion cell layer (GCL) is indicated in the uninjured sample. N= 3 fish per time point and uninjured controls. Scale bar: 30 µm. **(B)** Magnification of the areas indicated by the squares 1 and 2 in panel A. Scale bar: 10 µm.

Figure 5

A

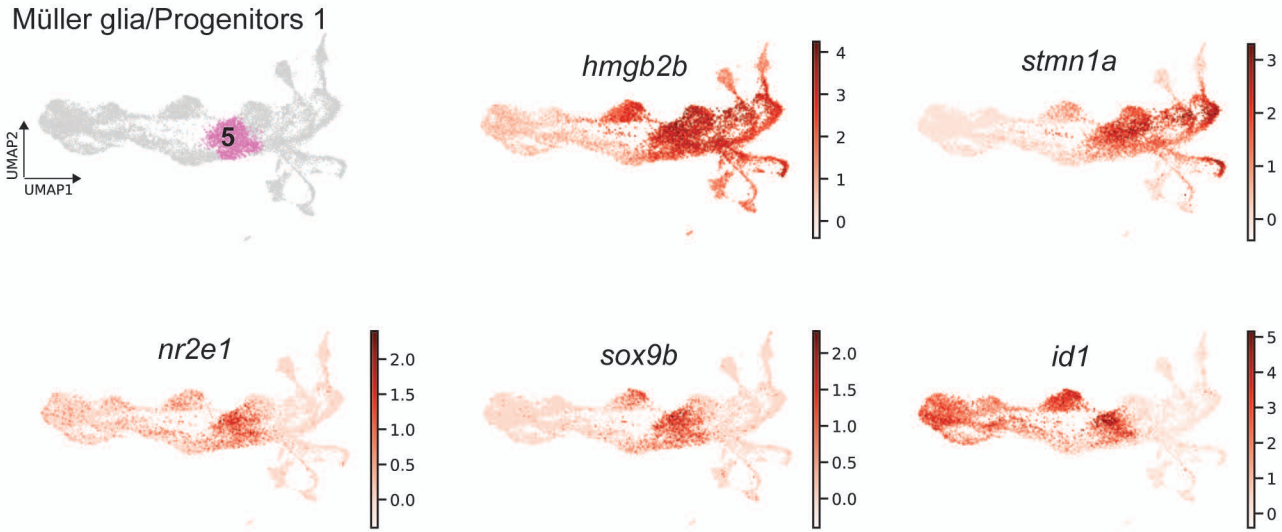
Müller glia/Progenitors 1
5
UMAP2
UMAP1
hmgb2b
4
3
2
1
0
stmn1a
3
2
1
0
nr2e1
2.0
1.5
1.0
0.5
0.0
sox9b
2.0
1.5
1.0
0.5
0.0
id1
5
4
3
2
1
0

B

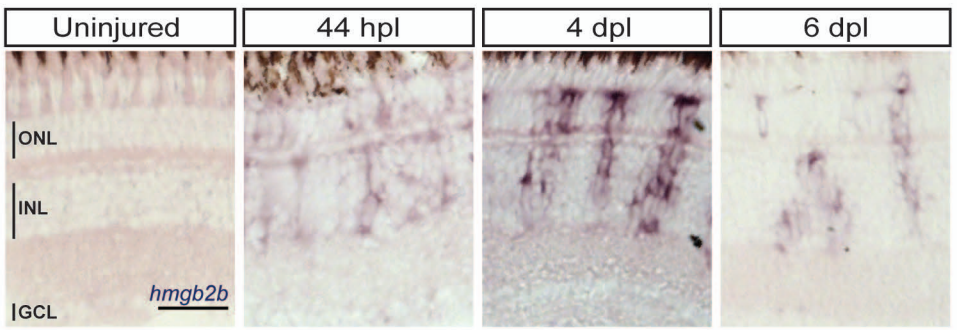
Uninjured
44 hpl
4 dpl
6 dpl
ONL
INL
GCL
hmgb2b

**Figure 5: scRNAseq identifies a transient cell population with hybrid characteristics of reactive Müller glia and early progenitors in the light-lesioned retina. (A)** The progenitor 1 cluster (cluster 5) and the expression levels of *hmgb2b*, *stmn1a*, *nr2e1 sox9b* and *id1*. **(B)** Bright field microscopy images of chromogenic *in situ* hybridization detecting *hmgb2b* on retinal sections of uninjured control animals and at 44 hours post lesion (hpl), 4 days post lesion (dpl) and 6 dpl. N= 3 fish per time point and uninjured controls. The position of the outer nuclear layer (ONL), inner nuclear layer (INL) and ganglion cell layer (GCL) is indicated in the uninjured sample. Scale bar: 30 µm.

Figure 6

A

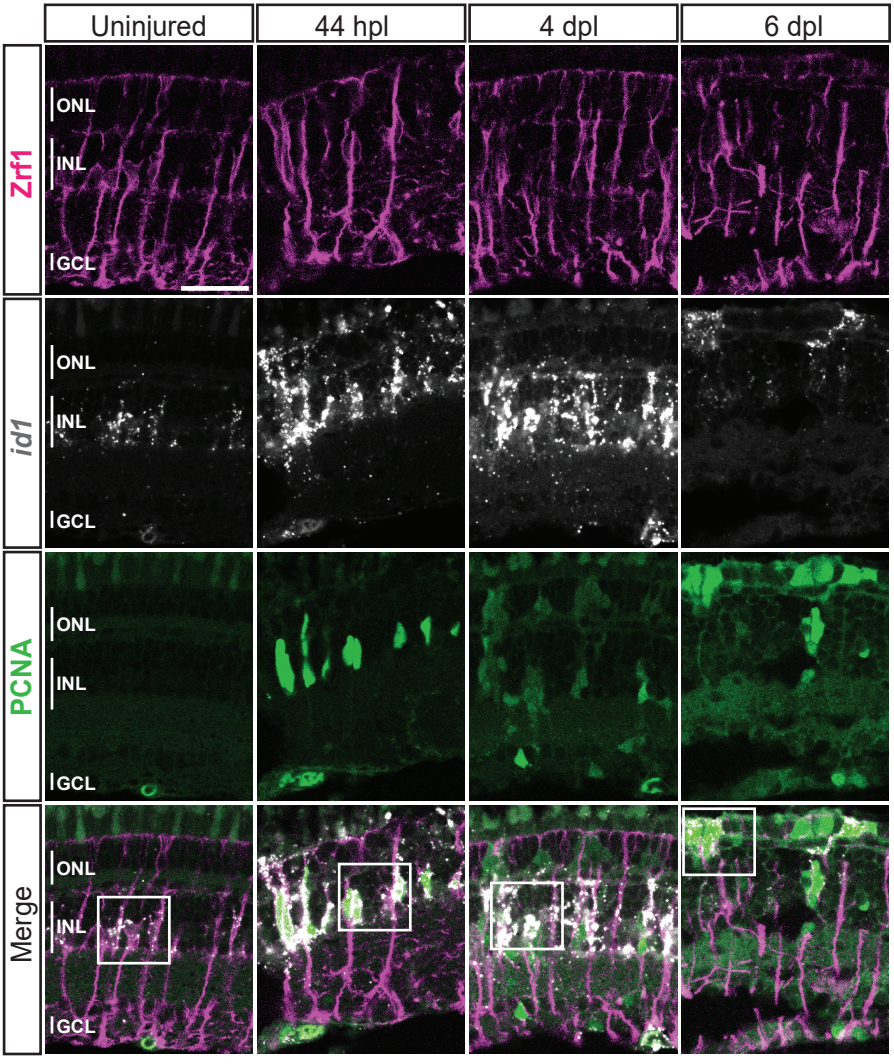
Uninjured
44 hpl
4 dpl
6 dpl
Zrf1
id1
PCNA
Merge
ONL
INL
GCL

B

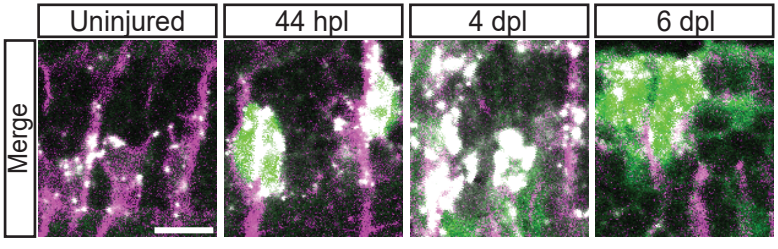
Uninjured
44 hpl
4 dpl
6 dpl
Merge

**Figure 6: expression profile of *id1* during retina regeneration. (A)** Confocal images of fluorescent *in situ* hybridization for *id1* (grey) and immunohistochemistry detecting Zrf1-positive MG fibers (magenta) and the proliferation marker PCNA (green) on retinal sections of uninjured control animals and at 44 hours post lesion (hpl), 4 and 6 days post lesion (dpl). The position of the outer nuclear layer (ONL), inner nuclear layer (INL) and ganglion cell layer (GCL) is indicated in the uninjured sample. N= 3 fish per time point and uninjured controls. Scale bar: 30 µm. **(B)** Magnification of the areas indicated by the squares 1 and 2 in panel A. Scale bar: 10 µm.

Figure 7

A

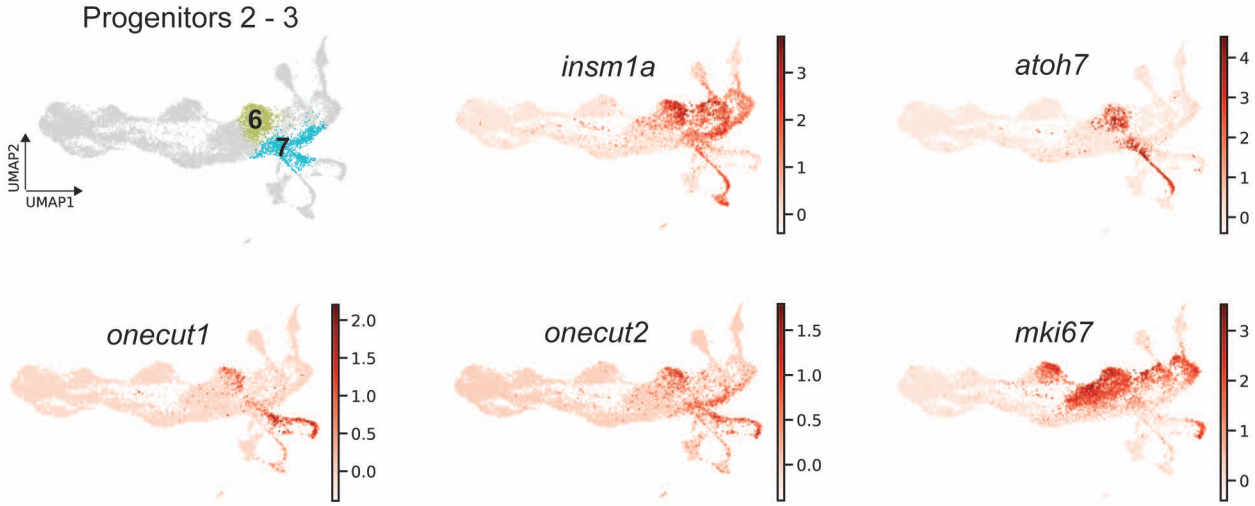
Progenitors 2 - 3
6
7
UMAP2
UMAP1
insm1a
3
2
1
0
atoh7
4
3
2
1
0
onecut1
2.0
1.5
1.0
0.5
0.0
onecut2
1.5
1.0
0.5
0.0
mki67
3
2
1
0

B

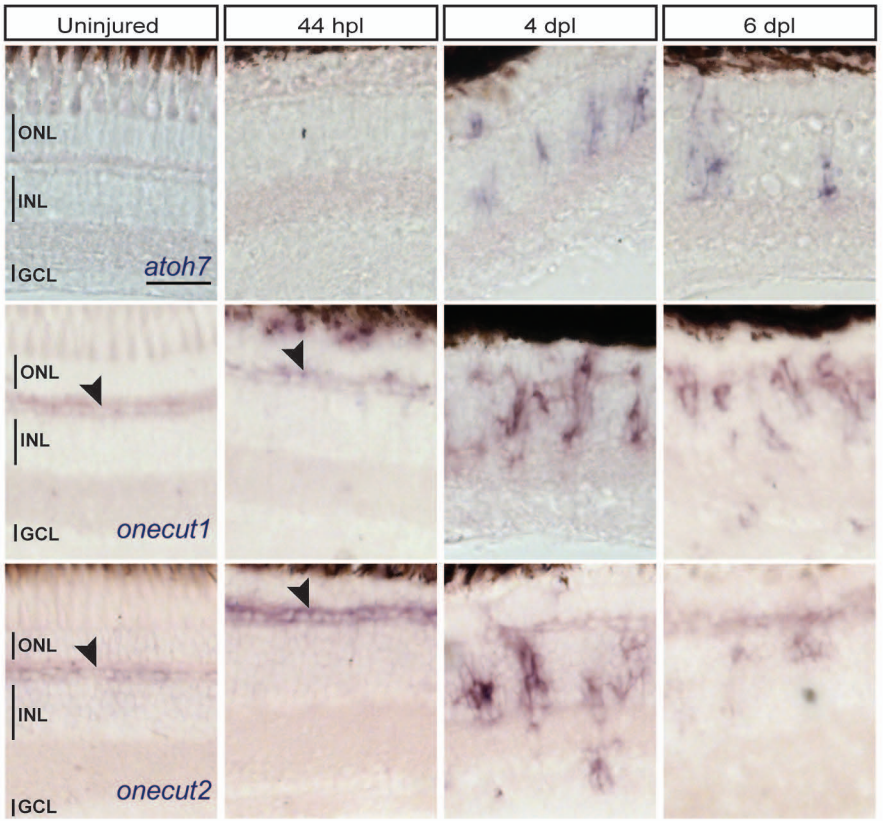
Uninjured
44 hpl
4 dpl
6 dpl
ONL
INL
GCL
atoh7
ONL
INL
GCL
onecut1
ONL
INL
GCL
onecut2

**Figure 7: scRNAseq identifies two neurogenic progenitor populations in the light-lesioned retina. (A)** The two progenitor clusters (cluster 6 and 7) and the relative expression levels of *insm1a*, *atoh7*, *onecut1*, *onecut2* and *mki67*. **(B)** Bright field microscopy images of chromogenic *in situ* hybridization detecting *atoh7*, *onecut1* or *onecut2* on retinal sections of uninjured control animals and at 44 hours post lesion (hpl), 4 days post lesion (dpl) and 6 dpl. Each ISH was carried on N= 3 fish per time point and uninjured controls.The position of the outer nuclear layer (ONL), inner nuclear layer (INL) and ganglion cell layer (GCL) is indicated in the uninjured sample. Scale bar: 30 µm.

Figure 8

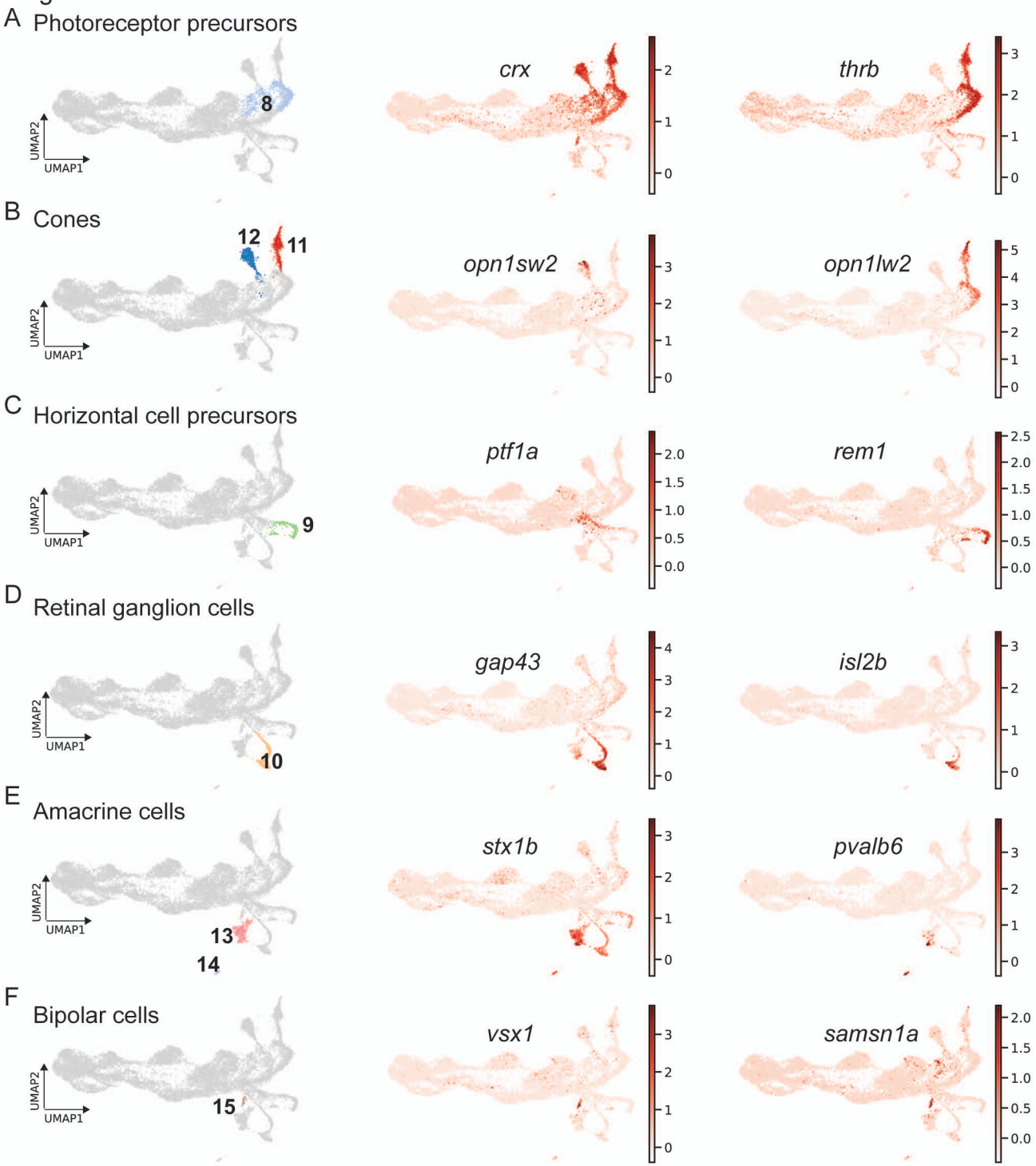
A
Photoreceptor precursors
8
crx
thrb
B
Cones
12
11
opn1sw2
opn1lw2
C
Horizontal cell precursors
9
ptf1a
rem1
D
Retinal ganglion cells
10
gap43
isl2b
E
Amacrine cells
13
14
stx1b
pvalb6
F
Bipolar cells
15
vsx1
samsn1a
UMAP1
UMAP2

**Figure 8: scRNAseq identifies fate-restricted progenitors and differentiating progeny in the light-lesioned retina. (A)** The photoreceptor precursor cluster (cluster 8) and the expression levels of *crx* and *thrb*. **(B)** The red and blue cone cluster (cluster 11 and 12) and the expression levels of the blue cone marker *opn1sw2* and red cone marker *opn1lw2*. **(C)** The horizontal cell precursor cluster (cluster 9) and the expression levels of *ptf1a* and *rem1*. **(D)** The ganglion cell cluster (cluster 10) and the expression levels of *gap43* and *isl2b*. **(E)** The two amacrine cell clusters (cluster 14 and 15) and the expression levels of *stx1b* and *pvalb6*. **(D)** The bipolar cell cluster (cluster 15) and the expression levels of the known bipolar cell marker *vsx1* and the novel marker *samsn1a*. **Associated: supplemental figure 1 and 2.**

Figure 9

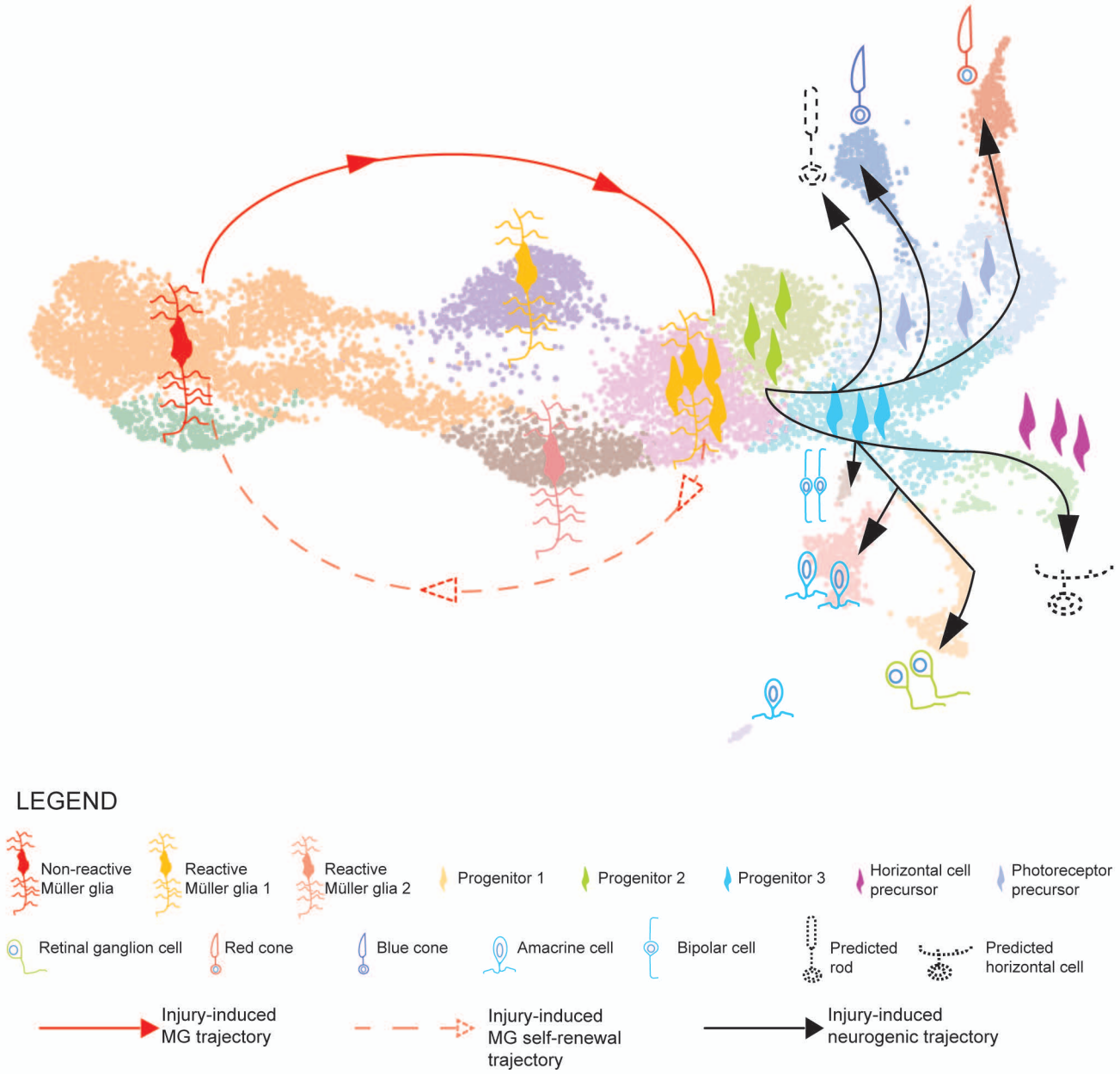
LEGEND
Non-reactive Müller glia
Reactive Müller glia 1
Reactive Müller glia 2
Progenitor 1
Progenitor 2
Progenitor 3
Horizontal cell precursor
Photoreceptor precursor
Retinal ganglion cell
Red cone
Blue cone
Amacrine cell
Bipolar cell
Predicted rod
Predicted horizontal cell
Injury-induced MG trajectory
Injury-induced MG self-renewal trajectory
Injury-induced neurogenic trajectory

**Figure 9: model summarizing the cellular events underlying retina regeneration in zebrafish.** Upon lesion, non-reactive MG on the left side of the main transcriptional UMAP feed into a hybrid Müller glia/progenitor population via reactive Müller glia (solid red line). Based from this hybrid cell population, we find a Müller glia trajectory reverting to the initial starting point indicating Müller glia self-renewal (dashed red line). Moreover, the hybrid cell population represents the tip of the neurogenic trajectory, resulting in the formation of neuronal precursors and differentiating neurons (solid black lines). Differentiating rods and horizontal cells, which have not been found in the scRNAseq, are indicated with dashed lines and positioned in the predicted location on the main UMAP.

Figure 1-figure supplement 1

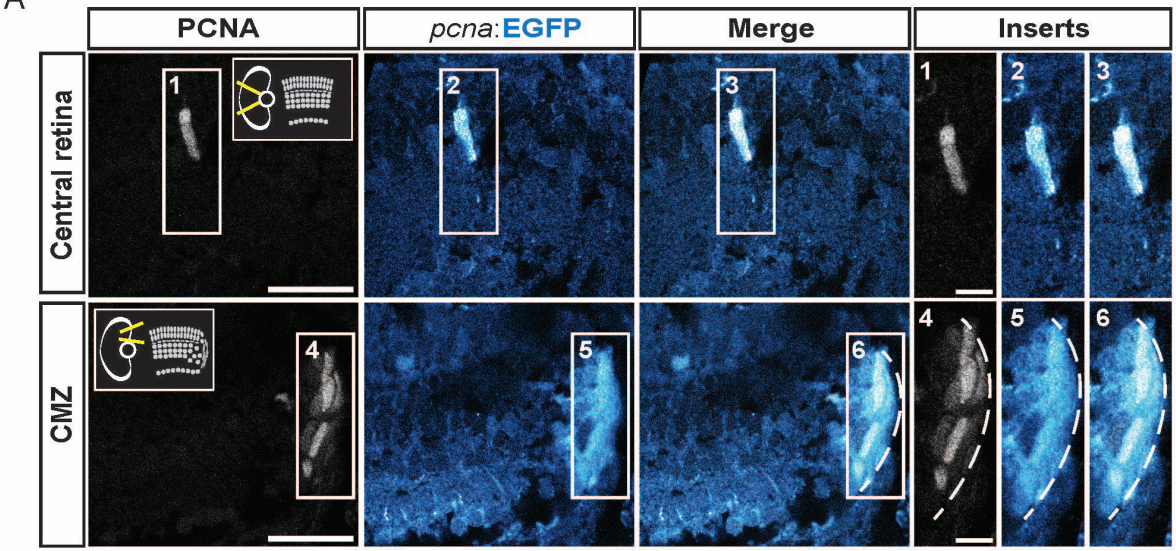


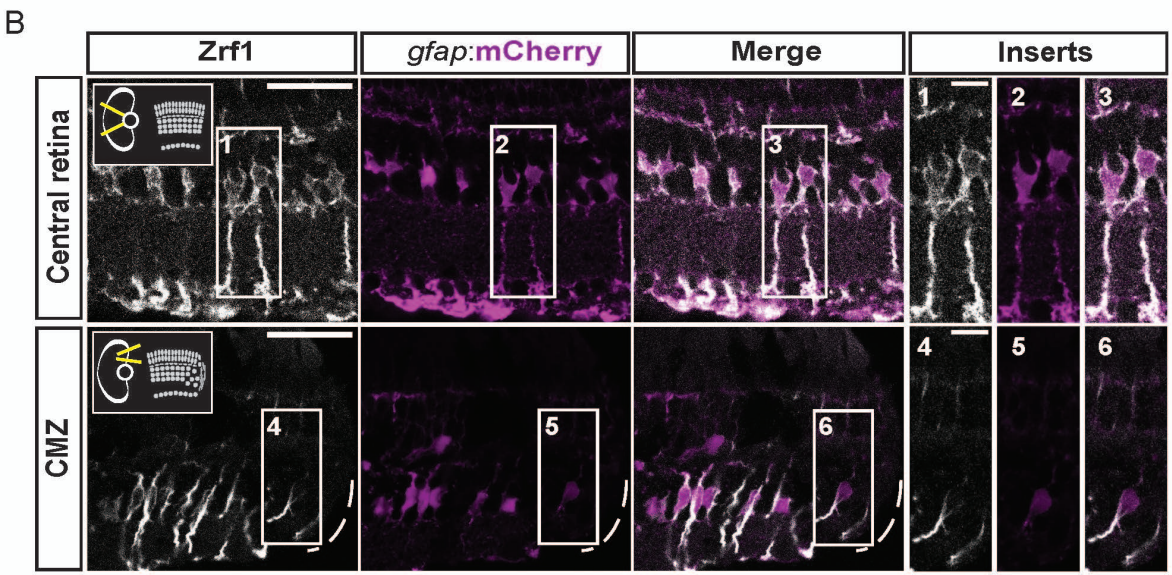

**Figure 1-figure supplement 1: characterization of the fluorescent reporter lines *Tg(pcna:EGFP)* and *Tg(gfap:mCherry)* in double transgenic animals. (A)** Confocal images of immunohistochemistry against the proliferation marker PCNA (grey) and EGFP (blue) on retinal sections of *Tg(pcna:EGFP);Tg(gfap:mCherry)* animals. Schemes in the thumbnails on the top-right and top-left of the PCNA panels indicate the region of interest, either the central retina or the ciliary marginal zone (CMZ). N= 3 fish. **(B)** Confocal images of immunohistochemistry detecting Zrf1-positive MG fibers (magenta) and mCherry on retinal sections of *Tg(pcna:EGFP);Tg(gfap:mCherry)* animals. N= 3 fish. Scale bar: 30 µm for main panels, 10 µm for inserts.

Figure 1-figure supplement 2

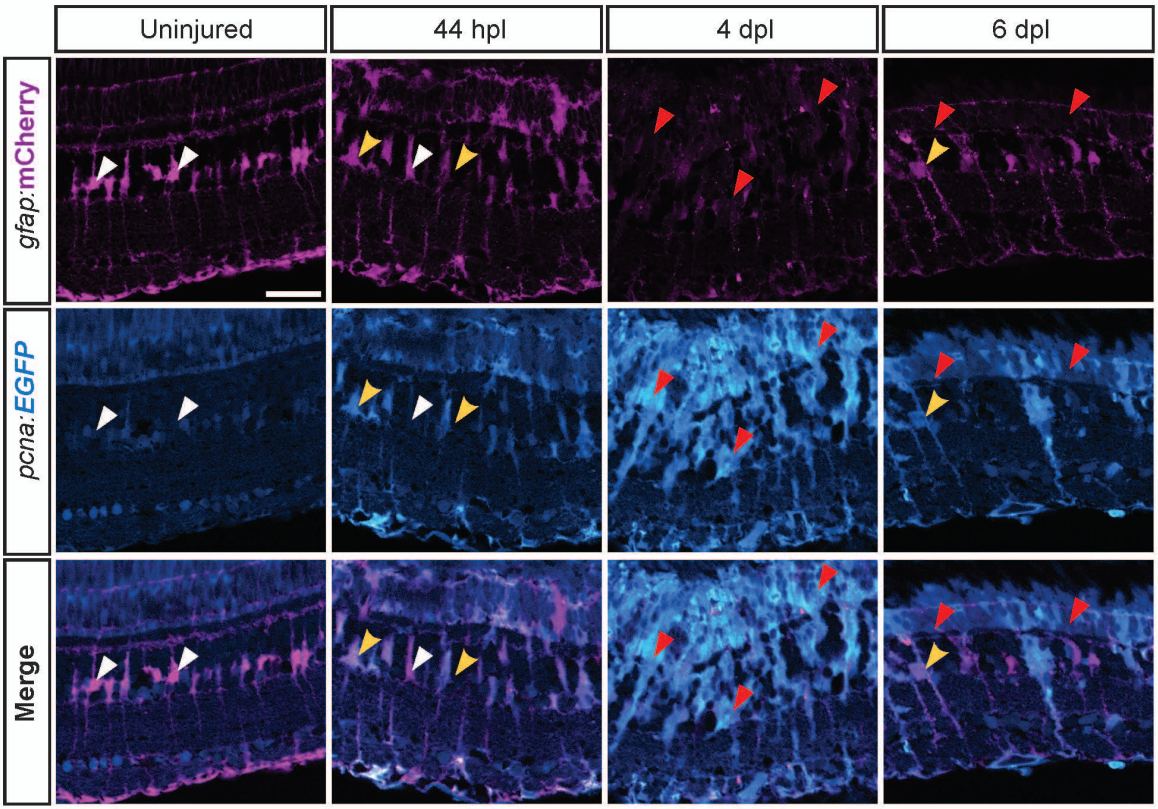

**Figure 1-figure supplement 2: expression profile of *Tg(pcna:EGFP);Tg(gfap:mCherry)* during retina regeneration.** Apotome images showing endogenous immunofluorescence of EGFP and mCherry driven by *Tg(pcna:EGFP)* and *Tg(gfap:mCherry)* on retinal sections in uninjured as well as lesioned conditions at different time points. White arrowheads indicate mCherry-positive, EGFP-negative MG. Yellow arrowheads indicate mCherry-/EGFP-double positive MG. Red arrowheads indicate low-mCherry-/EGFP-double positive, putative RPCs. N= 3 fish per time point and uninjured controls. Scale bar: 30 μm.

Figure 1-figure supplement 3

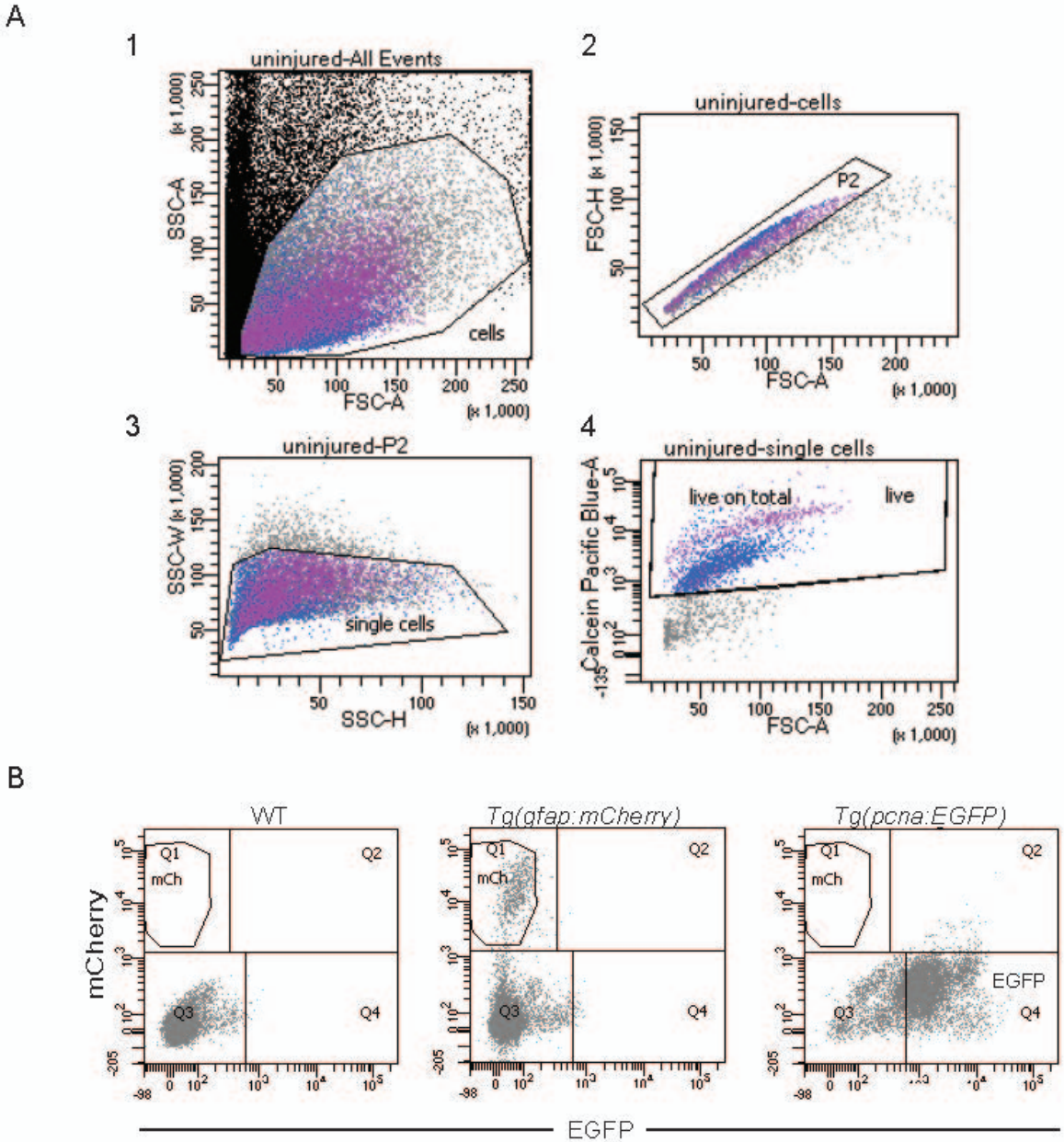

**Figure 1-figure supplement 3: fluorescence activated cell sorting (FACS) and gating strategies. (A)** Flow cytometry plots of dissociated, uninjured retinae from *Tg(pcna:EGFP);Tg(gfap:mCherry)* fish and gating strategy for sorting calcein-positive cells. Plot 1 displays all the events in a single cell suspension according to the forward (x axis) and side scatter (y axis) areas. Among cells gated in 1, singlets (P2) were chosen by considering the area (x axis) and the height (y axis) of the forward scatter in 2. Height (x axis) and width (y axis) of the side scatter were plotted in 3 to further gate singlets among P2. Finally, only calcein-positive (i.e. living) cells were gated among singlets in 4. The gating strategy was the same for the uninjured as well as all lesioned samples. Samples consisted of single cell suspensions derived from 8 retinae of 4 fish (2 males and 2 females) each. **(B)** Flow cytometry plots showing EGFP and mCherry fluorescence of cells from WT, *Tg(gfap:mCherry)* and *Tg(pcna:EGFP)* dissociated retinae.

Figure 2-figure supplement 1

A

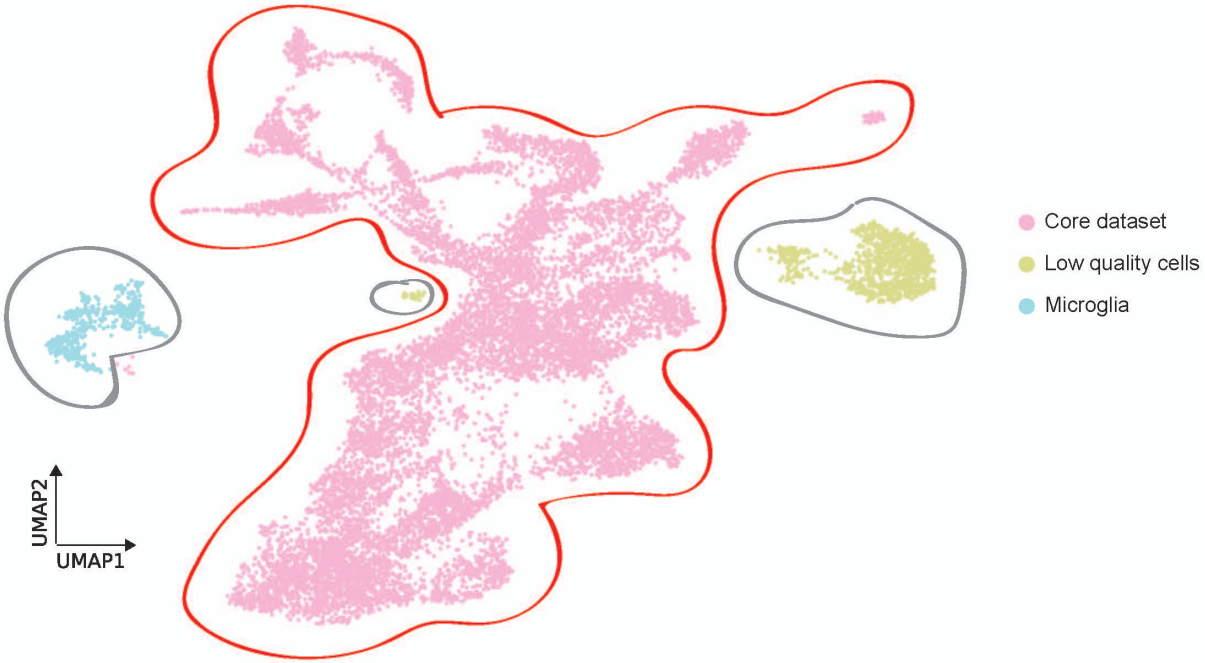


B

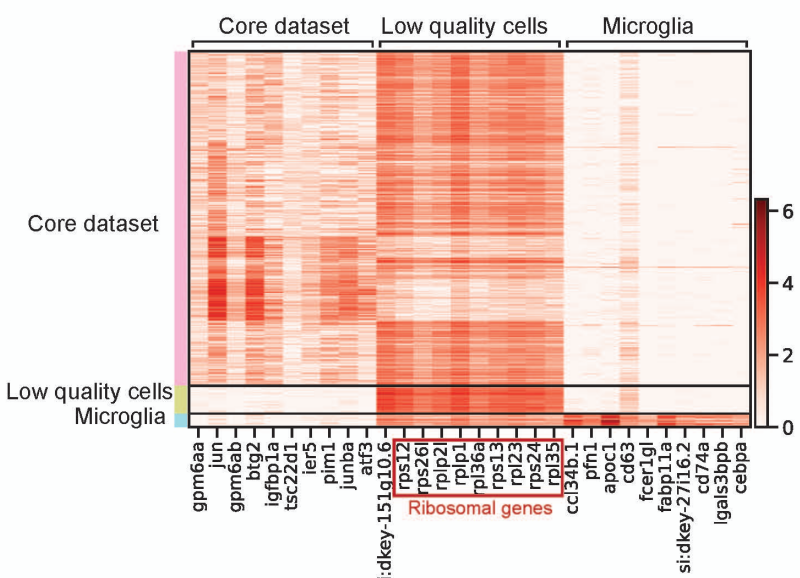

**Figure 2-figure supplement 1: original scRNAseq dataset.** **(A)** UMAP of the original scRNAseq dataset containing 13.139 cells and consisting of a core cluster (circled in red) and two clusters of microglia and low-quality cells (circled in grey). **(B)** Heat map depicting the expression of the top 10 marker genes per cluster of the original dataset.

# Figure 2-figure supplement 2

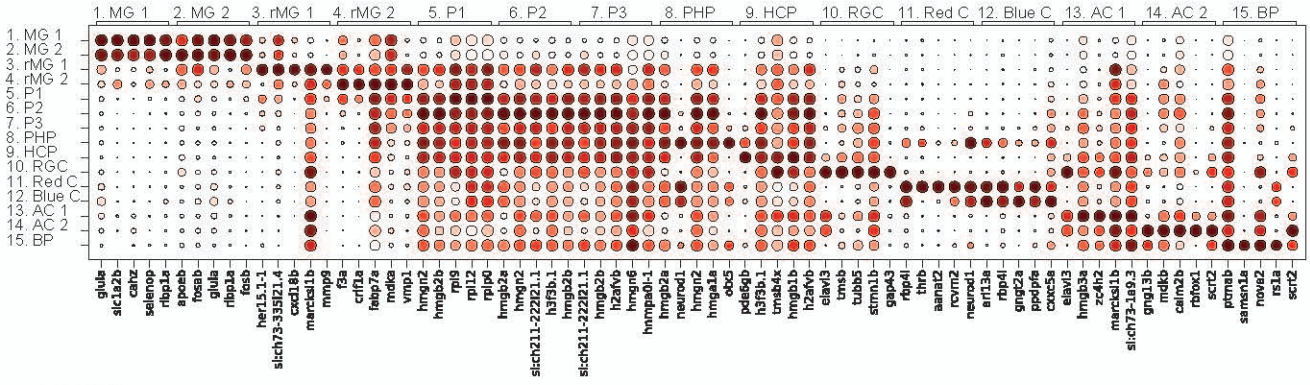


LEGEND

MG 1 = Non-reactive Müller glia 1
MG 2 = Non-reactive Müller glia 2
rMG 1 = Reactive Müller glia 1
rMG 2 = Reactive Müller glia 2
P1 = Müller glia/Progenitors 1
P2 = Progenitors 2
P3 = Progenitors 3
PHP = Photoreceptor precursors
HCP = Horizontal cell precursors
RGC = Retinal ganglion cells
Red C = Red cones
Blue C = Blue cones
AC 1 = Amacrine cells 1
AC 2 = Amacrine cells 2
BP = Bipolar cells

**Figure 2-figure supplement 2: dot plot of top 5 marker genes per cluster.** Dot plot depicting the expression of top 5 marker genes per cluster (see Figure 2A). Dot size scales with a fraction of cells expressing the gene, and the dot colour indicates the scaled mean gene expression in the cluster.

Figure 3-figure supplement 1

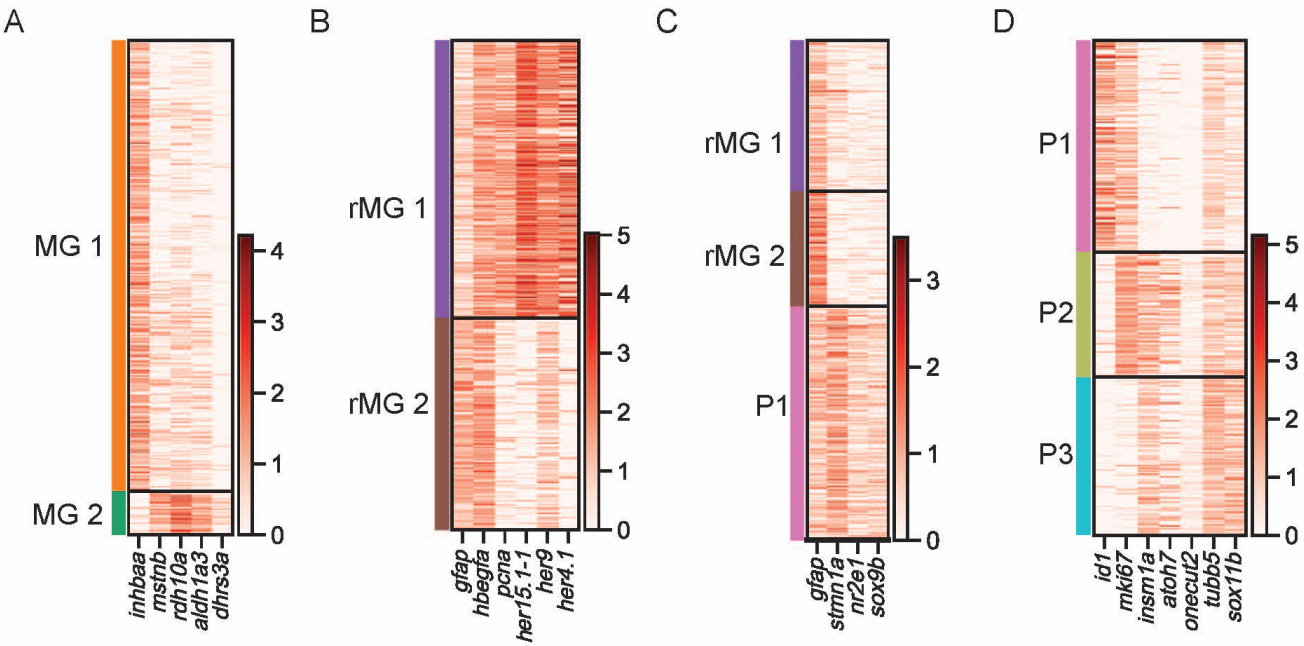


LEGEND

1. MG 1 = Non-reactive Müller glia 1
2. MG 2 = Non-reactive Müller glia 2
3. rMG 1 = Reactive Müller glia 1
4. rMG 2 = Reactive Müller glia 2
5. P1 = Müller glia/Progenitors 1
6. P2 = Progenitors 2
7. P3 = Progenitors 3

**Figure 3-figure supplement 1: expression of selected genes per cluster. (A)** Heat map showing differentially expressed genes between non-reactive MG 1 and non-reactive MG 2. **(B)** Heat map showing differentially expressed genes (*gfap, pcna, her15.1-1, her9, her4.1*) as well as shared (*hbegfa*) genes between reactive MG 1 and reactive MG 2. **(C)** Heat map showing differentially expressed genes in reactive MG1, reactive MG2 and P1. **(D)** Heat map showing differentially expressed genes in P1, P2 and P3.

Figure 8-figure supplement 1

A

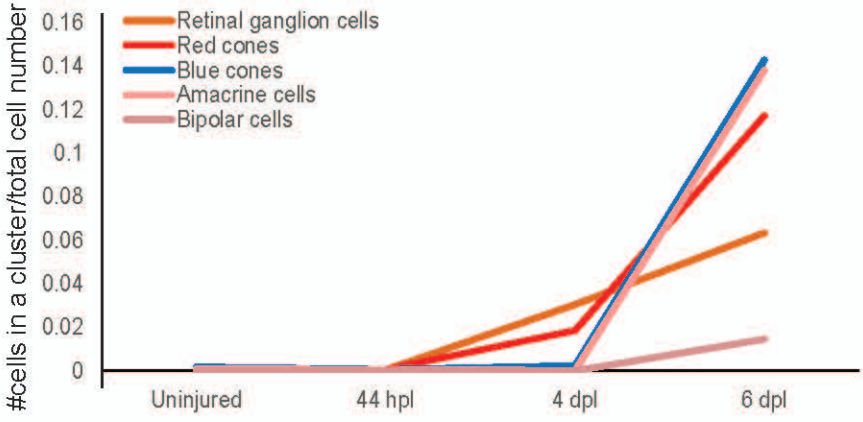

**Figure 8-figure supplement 1: birthdate order of regenerated progeny.** Graph plotting the fraction of cells (y-axis) embarking on a specific retinal cell fate (coloured curves) in relation to a given time point (x-axis). Total number of cells per condition: uninjured= 2243, 44 hpl= 1723, 4 dpl= 4899, 6 dpl= 2825.

Figure 8-figure supplement 2

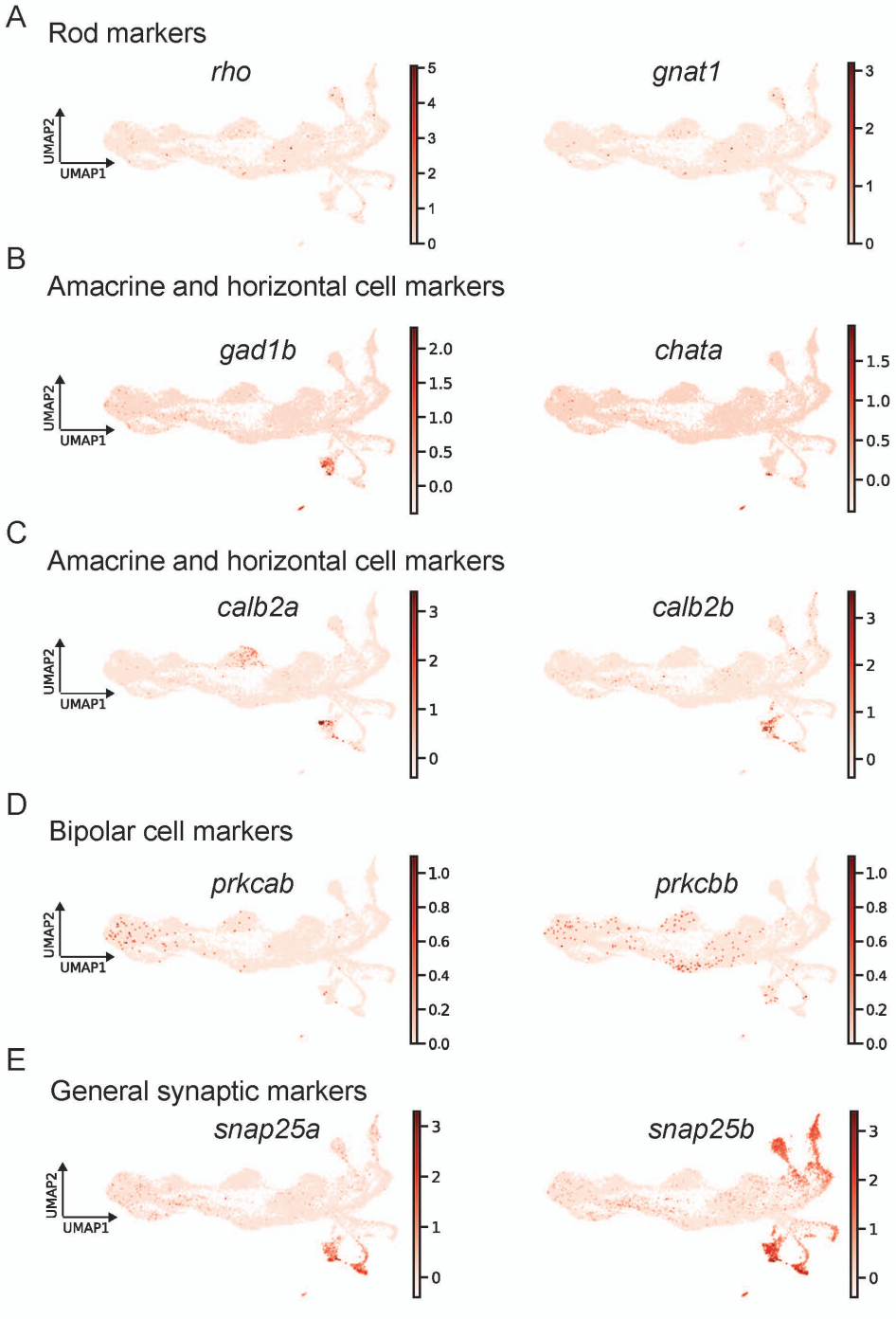

**Figure 8-figure supplement 2: expression of mature markers.** **(A)** Expression levels of the known rod markers *rho* and *gnat1*. **(B)** Expression levels of the known mature amacrine and horizontal cell markers *gad1b* and *chata*. **(C)** Expression levels of the known mature amacrine cell and horizontal cell markers *calb2a* and *calb2b*. **(D)** Expression levels of the known mature bipolar cell markers *prkcab* and *prkcbb*. **(E)** Expression levels of the general synaptic markers *snap25a* and *snap25b*.